REPORT DOCUMENTATION PAGE

Form Approved
OMB No. 0704-0188

1. AGENCY USE ONLY (Leave blank)	2. REPORT DATE	3. REPORT TYPE AND DATES COVERED
		FINAL REPORT 01 Sep 92 - 31 Aug 95

4. TITLE AND SUBTITLE
Scattering Absorption, and Generation of Microwaves in Time Varying and Structured Plasmas

5. FUNDING NUMBERS
3484/S3
611[illegible]D

6. AUTHOR(S)
Professor Spencer Kuo

7. PERFORMING ORGANIZATION NAME(S) AND ADDRESS(ES)
Weber Research Institute and Dept of Electrical Engineering
Polytechnic University
Route 110
Farmingdale, NY 11735

8. PERFORMING ORGANIZATION REPORT NUMBER

9. SPONSORING / MONITORING AGENCY NAME(S) AND ADDRESS(ES)
AFOSR/NE
110 Duncan AVenue Suite B115
Bolling AFB DC 20332-0001

10. SPONSORING / MONITORING AGENCY REPORT NUMBER
F49620-92-J-0349

11. SUPPLEMENTARY NOTES

AFOSR-TR-95
0790

12a. DISTRIBUTION / AVAILABILITY STATEMENT
APPROVED FOR PUBLIC RELEASE DISTRIBUTION UNLIMITED

13. ABSTRACT *(Maximum 200 words)*

The area of investigation of Mr James Faith is primarily on with the scattering and generation of microwaves by a spatially periodic and rapidly time varying plasma. The results indicate that this plasma device works as a dc to ac converter. Ms Ruthie Lyle is the other student supported by the DOD AASERT program. Her research deals with the potential application of plasma electromagnetic absorption and scattering for shielding objects from detection by conventional radar systems. A quasi-particle theory based on Wigner distribution function has been developed to study wave propagation and scattering in a periodically structured plasma.

14. SUBJECT TERMS			15. NUMBER OF PAGES
			16. PRICE CODE
17. SECURITY CLASSIFICATION OF REPORT	18. SECURITY CLASSIFICATION OF THIS PAGE	19. SECURITY CLASSIFICATION OF ABSTRACT	20. LIMITATION OF ABSTRACT
UNCLASSIFIED	UNCLASSIFIED	UNCLASSIFIED	

Polytechnic
UNIVERSITY

Technical Final Report
on
"Scattering, Absorption, and Generation of Microwaves in Time Varying and Structured Plasmas

Submitted by:

Professor Spencer Kuo, Principal Investigator

James Faith, Research Fellow
Ruthie Lyle, Research Fellow

Weber Research Institute and Department of Electrical Engineering
Polytechnic University
Route 110, Farmingdale, NY 11735

Prepared For
Air Force Office of Scientific Research
Grant No. AFOSR-F49 620-92-J-0349
September 1992 to August 31, 1995

Technical Final Report
on
"Scattering, Absorption, and Generation of Microwaves in Time Varying and Structured Plasmas

Submitted by:

Professor Spencer Kuo, Principal Investigator

James Faith, Research Fellow
Ruthie Lyle, Research Fellow

Weber Research Institute and Department of Electrical Engineering
Polytechnic University
Route 110, Farmingdale, NY 11735

Prepared For
Air Force Office of Scientific Research
Grant No. AFOSR-F49 620-92-J-0349
September 1992 to August 31, 1995

I. Introduction

Starting in September 1992, the DoD AASERT program has provided a three year augmentation award (AFOSR-F49620-92-J-0349) to the PI for training two graduate students to perform scientific research in conjunction with the PI's ongoing research activities: "Scattering, Absorption and Generation of Microwaves in time varying and structured plasmas" then sponsored by grant AFOSR-91-0002, and currently by the grant AFOSR-F49 670-94-0076. During the past three years, the two students Mr. James Faith and Ms. Ruthie Lyle have made significant progress in both academic area (coursework) and research area (carrying out research projects) for their thesis dissertations. Both have passed the area examination, and have completed all required coursework, are now in the final stage of their Ph.D. thesis work. Contained in this report are the works completed so far. Their theses representing the completed final report will be finished in a few months and will be submitted to amend the present report.

The two students' research involves two aspects of microwave-plasma interaction. The area of investigation of Mr. James Faith is primarily on with the scattering and generation of microwaves by a spatially periodic and rapidly time varying plasma. The plasma is produced by a nanosecond (nS) dc discharge through six pairs of equally spaced parallel electrodes. The results indicate that this plasma device works as a dc to ac converter. A wideband microwave pulse is produced during each discharge. The main goal of this work is to use such a fast growing plasma to upshift the frequency of an incident CW microwave from an external source. It turns out that an unexpected downshift process is observed. The downshifted line is trapped in the periodic plasma in a way similar to the trapping of an optical signal in a band gap of a periodic dielectric medium. Computer simulations have confirmed this observation. James has also worked on nonlinear wave particle interaction which leads to chaos in the particle trajectory. This work is enclosed in the appendix.

Ms. Ruthie Lyle (a very motivated African American woman, a very rare candidate in the engineering area) is the other student supported by the DoD AASERT program. Her research deals with the potential application of plasma electromagnetic absorption and scattering for shielding objects from detection by conventional radar systems. A quasi-particle theory based on Wigner distribution function has been developed to study wave propagation and scattering in a periodically structured plasma This theory includes the

effect of multiple scattering and is applicable in the cases of interest. Ruthie has applied the theory to study the ionospheric scintillation phenomena. Her analysis includes the spectral bandwidth effect of ionospheric density irregularities on the scintillation results.

II. Publications

Journal Articles:

1. James Faith, S.P. Kuo, and Joe Huang, "Chaotic Electron Motion Driven by Whistler Waves in the Magnetosphere", accepted for publication in *Comments on Plasma Physics and Controlled Fusion.*

2. James Faith, S.P. Kuo, and Joe Huang, "Electron Precipitation Caused by Chaotic Motion in the Magnetosphere due to Large Amplitude Whistler Waves", submitted to *Journal of Geophysical Research.*

Proceedings Issued Articles:

1. James Faith, S.P. Kuo, and Joe Huang, "Chaotic Electron Motion Driven by Whistler Waves in the Magnetosphere", *International Conference on Phenomena in Ionized Gas, August,* 1995, Hoboken, NJ.

2. Ruthie Lyle, "The Spectral Effect of the Ionospheric Irregularities on the Scintillation of Transionospheric Signals", *International Conference on Phenomena in Ionized Gas, August,* 1995, Hoboken, NJ.

Conference Presentations:

1. J. Kim, J. Faith, S.P. Kuo, "Design of a High Harmonic Cusptron Oscillator of an Inverted Configuration", *APS Annual Meeting of Plasma Science,* 11/16-11/18, 1992, Seattle, WA.

2. J. Kim, J. Faith, and S. P. Kuo, "Numerical Simulation for High Harmonic Inverted Cusptron Devices", *IEEE International Conference on Plasma Science,* 6/7-6/9, 1993, Vancouver, Canada.

3. J. Faith, J. Kim, S.P. Kuo, "Design of High Harmonic Inverted Cusptron Device", *APS Annual Meeting of Plasma Science,* 11/1-11/5, 1993, St. Louis, MO.

4. S.P. Kuo, J. Kim, J. Faith, "Design of High Harmonic Inverted Cusptron Device", *DoD Advisory Group on Electron Devices Conference*, 5/10-5/12, 1994, Monterey, CA.

5. J. Faith and S.P. Kuo, "Generation of ELF and VLF Waves in the HF Heater-Modulated Polar Electrojet", *IEEE International Conference on Plasma Science,* 6/6-6/8, 1994, Sante Fe, NM.

6. J. Kim, J. Faith, S.P. Kuo, "High Harmonic Cusptron Device with an Inverted Structure", *IEEE International Conference on Plasma Science,* 6/6-6/8, 1994, Sante Fe, NM.

7. J. Faith, S.P. Kuo, J. Sun, J. Huang, "Experimental Study of Frequency Shift of an Electromagnetic Wave Propagating Through a Rapidly Created Periodic Plasma", *APS Annual Meeting of Plasma Science,* 11/7-11/11, 1994, Minneapolis, MN.

8. J. Sun, J. Huang, S.P. Kuo, J. Faith, "Simulation Study on Electromagnetic Frequency Shift in Rapidly Created and Periodically Structured Plasma", *APS Annual Meeting of Plasma Science,,* 11/7-11/11, 1994, Minneapolis, MN.

9. Ruthie Lyle, J. Huang, and S.P. Kuo, "Electromagnetic Wave Scattering in an Inhomogeneous Plasma Characterized by Periodic Structure", *APS Annual Meeting of Plasma Science,,* 11/7-11/11, 1994, Minneapolis, MN.

10. J. Faith, J. Huang, S.P. Kuo, "Experimental Study of Frequency Shift of an Electromagnetic Wave Propagating Through a Rapidly Created Periodic Plasma", *IEEE International Conference on Plasma Science,* 6/5-6/8, 1995, Madison, WI.

11. J. Faith, J. Huang, S.P. Kuo, "Experimental Study of the Conversion of DC Electric Fields to Microwave radiation by an Ionization Front Created by Successive Discharges" *IEEE International Conference on Plasma Science,* 6/5-6/8, 1995, Madison, WI.

12. J. Huang, J. Faith, S.P. Kuo, "Chaotic Particle Motion in Large Amplitude Whistler Wave in the Magnetosphere", *IEEE International Conference on Plasma Science,* 6/5-6/8, 1995, Madison, WI.

13. Ruthie Lyle, S.P. Kuo, and J. Huang, "Study of Electromagnetic Wave Scattering by Periodic Density Irregularities in Plasma", *IEEE International Conference on Plasma Science,* 6/5-6/8, 1995, Madison, WI.

14. J. Huang, S.P. Kuo, and James Faith, "Multiple Frequency Conversion of an Electromagnetic Wave Interacting with a Rapidly Created Periodic Plasma", *APS Annual Meeting on Plasma Science,* 11/6-11/10, 1995, Louisville, KY.

15. S.P. Kuo, James Faith, and J. Huang, "Frequency Shift of an Electromagnetic Wave Interacting with a Rapidly Created Periodic Plasma", *APS Annual Meeting on Plasma Science,* 11/6-11/10, 1995, Louisville, KY.

16. J. Faith, Joe Huang, and S.P. Kuo, "Experiment on the Conversion of dc Electric Fields to Radiation by Successive Discharges", *APS Annual Meeting on Plasma Science,* 11/6-11/10, 1995, Louisville, KY.

17. James Faith, S.P. Kuo, Joe Huang, "Chaotic Electron Motion Driven by Whistler Waves in the Magnetosphere", *APS Annual Meeting on Plasma Science,* 11/6-11/10, 1995, Louisville, KY.

18. Ruthie Lyle, S.P. Kuo, and J. Huang, "Spectral Effect of Ionospheric Irregularities on Scintillation of Transionospheric Signals", *APS Annual Meeting on Plasma Science,* 11/6-11/10, 1995, Louisville, KY.

19. James Faith, S.P. Kuo, and Joe Huang ,"Electron Precipitation caused by Chaotic Electron Motion in the Magnetosphere due to Large Amplitude Whistler Waves", *National Radio Science Meeting,* 1/9-1/13, 1995, Boulder, CO.

20. Ruthie Lyle, S.P. Kuo, and J. Huang, "Spectral Effect of Ionospheric Irregularities on the Scintillation of Transionospheric Signals", *National Radio Science Meeting,* 1/9-1/13, 1995, Boulder, CO.

III. Summary of the Works Completed

A. Scattering of Microwaves by a Rapidly Produced Spatially Periodic Plasma

Recently, there has been a considerable interest in the study of the propagation of an electromagnetic wave through a plasma whose density profile changes rapidly in time. It is motivated by the fact that a plasma device may be devised to tune the frequency of existing sources of microwaves or to convert a CW source wave into a wideband pulse

train, where the period of the pulse train and the length of each pulse are determined by the repetition rate of the plasma discharge and the length of the plasma volume respectively. Such a wideband pulse train has a potential application as a radar jamming source

Theory and numerical simulation on this wave frequency shift by interacting with a suddenly created uniform plasma have been performed. Several experiments confirming the theoretical predictions have been carried out. In those works, a plasma slab (with plasma frequency ω_{pe}) is used to convert the preexisting electromagnetic wave (with frequency ω_0) to an upshifted frequency $(\omega_0^2+\omega_{pe}^2)^{1/2}$. The physical mechanism can be simply explained as follows. Since the plasma slab is generated suddenly in time, the wave does not experience any spatial variation inside the slab, and therefore the wavelength of the wave will not change. The wave in the new medium has to satisfy the new dispersion relation $\omega^2=\omega_{pe}^2+k_0^2c^2$ and $k_0=\omega_0/c$, thus its frequency ω is upshifted from the initial value $\omega_0=k_0c$ to the new value $\omega=(\omega_0^2+\omega_{pe}^2)^{1/2}$

In the present work we consider the case of a wave propagating through periodically spaced suddenly generated plasma slabs. The frequency shift phenomena in this case becomes much more complicated since the wave k_0 can now interact with the structure $k_p$of the plasma and different Floquet modes of the periodic structure can be excited. Therefore, a number of frequencies are expected to emerge due to the temporal discontinuity a periodically spatial discontinuity the wave experiences. The result of this scattering phenomena can be concisely represented in a band diagram of the dispersion curve similar to that encountered in solid state physics. This curve compared to that for a uniform plasma shows that pass bands emerge in the cutoff frequency regime while the stop bands (band gaps) appear in the propagating frequency regime. Therefore both upshifted and downshifted signals are expected to be generated as the initial wave interacts with such a suddenly created periodic plasma. The experiment has been performed to confirm the theoretical predictions.

We have constructed a chamber experiment to investigate the frequency shifting of an CW microwave. The experiment consists of a pair of electrodes, each consisting of an aluminum sheet in which eleven 3cm slots have been cut, with 3cm between each slot. These are backed with a solid copper sheet which provides an effective waveguide for the

incident wave. In each of the depressions created by the slots in the aluminum we arrange many metal spikes. The discharge will occur only in the region where the spikes are present (as opposes to arcing from the corners of the electrodes), due to the large electric fields at the tips. A photograph of the discharge is shown in Fig. 1. These electrode structures are placed facing one another within a vacuum chamber (dimensions: 2½'×1½'×1') constructed of 1" Plexiglas. When evacuated to low pressure (~0.5 Torr) we rapidly create a plasma between the electrodes by discharge from a Marx capacitor bank. The CW microwave is fed into one end of the chamber with an S band horn antenna, and the received signal is collected by another horn of the appropriate band at the other end. The results of several hundred discharges are collected on our HP 8105 spectrum analyzer and downloaded to a PC for storage. A schematic of the experimental setup is shown in Fig. 2.

We have investigated two cases experimentally. In the first, the incident frequency is chosen to be 4GHz, and the discharge 75 kV, such that $\omega>\omega_p$. In this case the dominant spectral features are up-shifted, to be discussed in the theory below. We find an upshifted peak at 7.5 GHz, which is a greater relative shift than that obtained by a single slab plasma. This result is presented in Fig. 3. It should be noted that in this case the conversion efficiency is very low. In the second experimental case investigated, incident frequency of 3.05 GHz and a 100 kV discharge with $\omega<\omega_p$, we encountered some new results, unexpected for a uniform plasma slab. We find that the dominant new wave can be trapped between the plasma layers and its downshifted peak at 2.5 GHz. As shown in Fig. 4. What is noted that there is a tremendous improvement in the conversion efficiency, with the downshifted peak 15 dB down from the incident wave. This represents about a 30 dB improvement over the largest upshifted peak we have observed (e.g. Fig. 3).

The experimental results can be understood qualitatively by using the Floquet theory. It is done by considering a wave of the type:

$$\Psi(z)=\begin{cases} A\exp[ik_0(1-\omega_p^2/\omega^2)^{1/2}z]+B\exp[-ik_0(1-\omega_p^2/\omega^2)^{1/2}z] & \text{inside the slabs} \\ C\exp[ik_0(z-L)]+D\exp[-ik_0(z-L)] & \text{outside the slabs} \end{cases},$$

where L is the periodicity, d is the slab width, and $k_0=2\pi/\lambda_0$ is the free space wavenumber. Applying the boundary conditions on Ψ and its derivative, along with the Bloch wave condition:

$$\Psi(z)=\exp[-i\beta L]\Psi(z+L)$$

we can find the dispersion relation for the wave propagating in the periodic plasma as:

Figure 1 A photograph of the discharge.

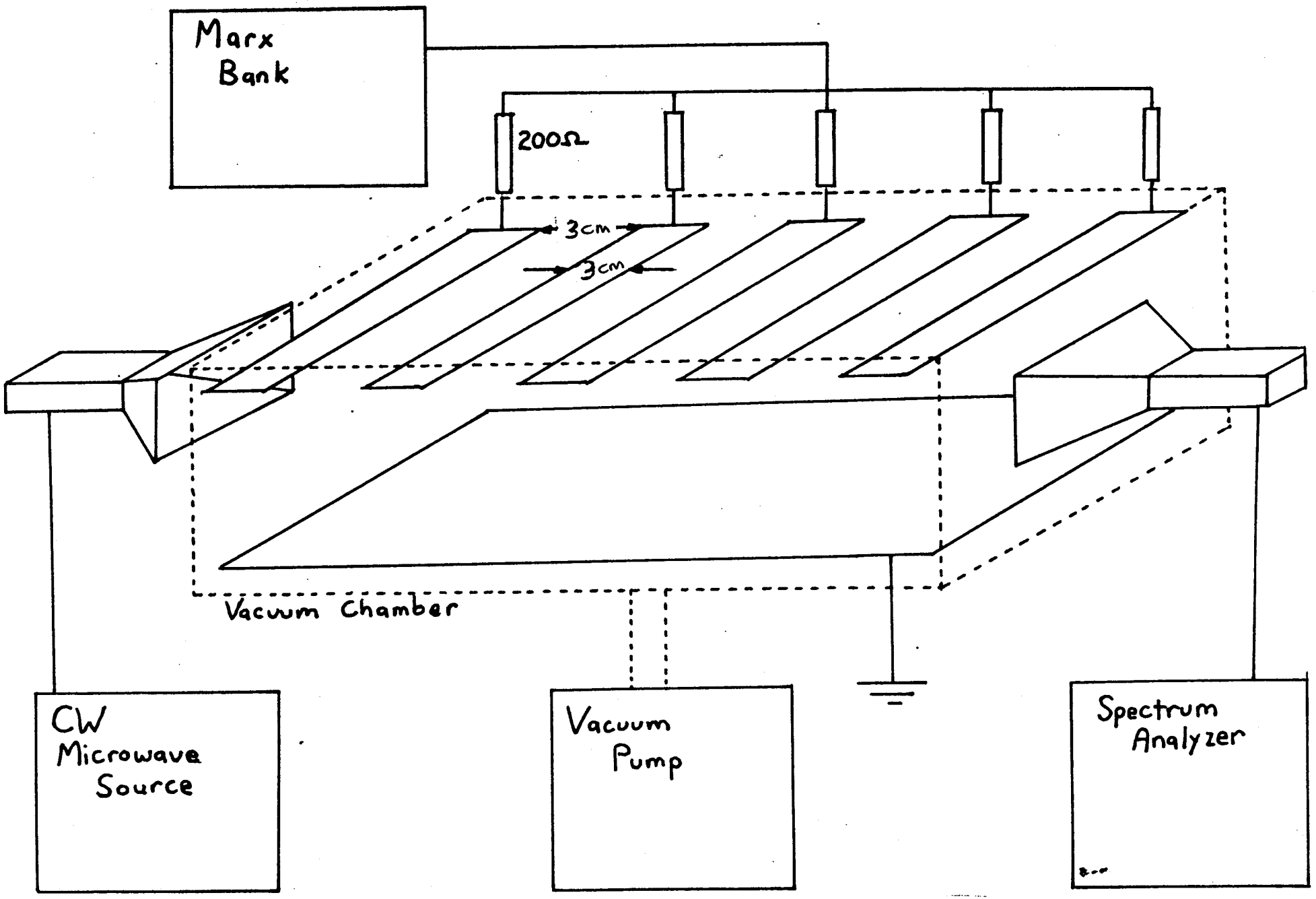

Figure 2 A schematic of the experimant.

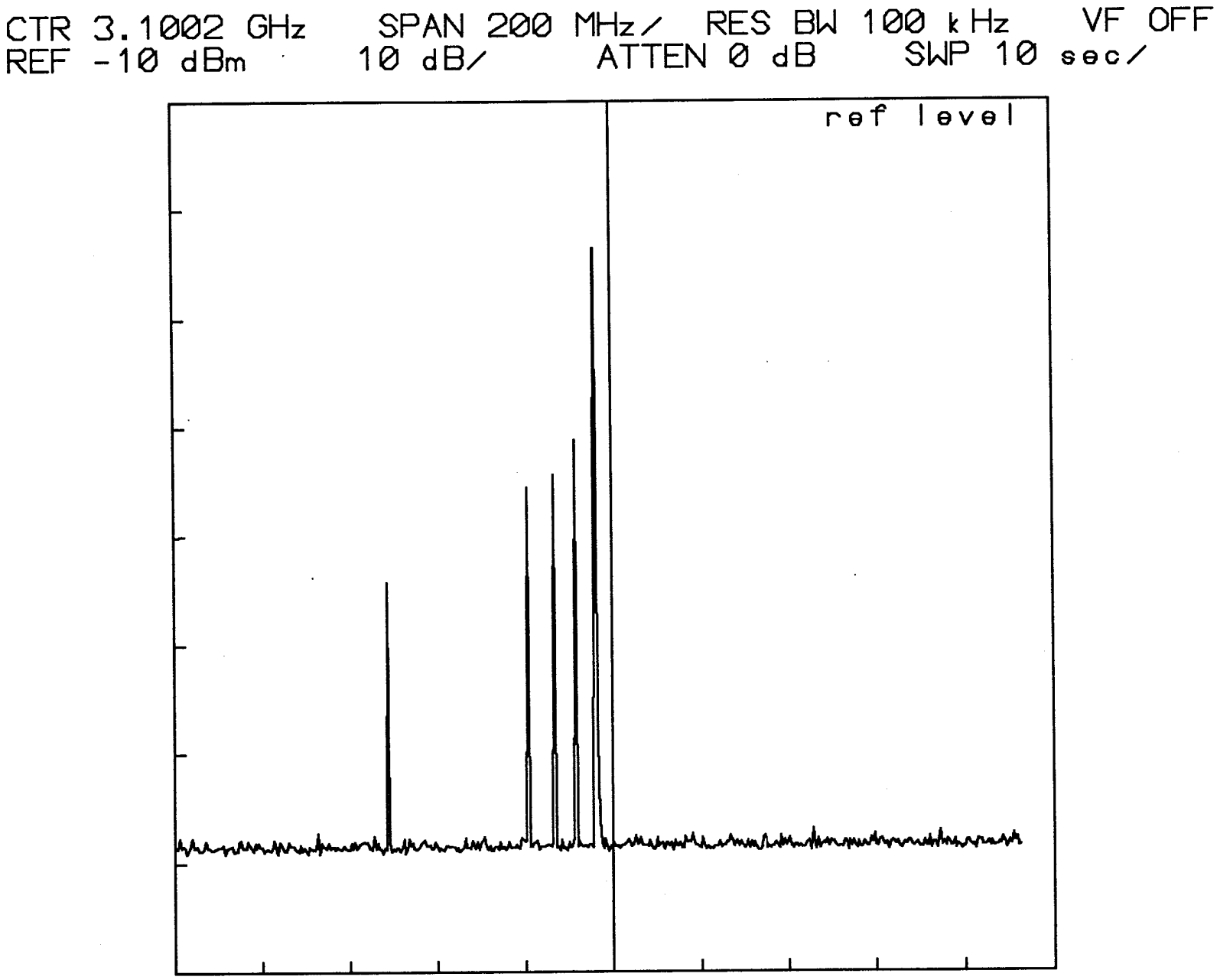

Figure 3 The experimantally observed down shifted peak.

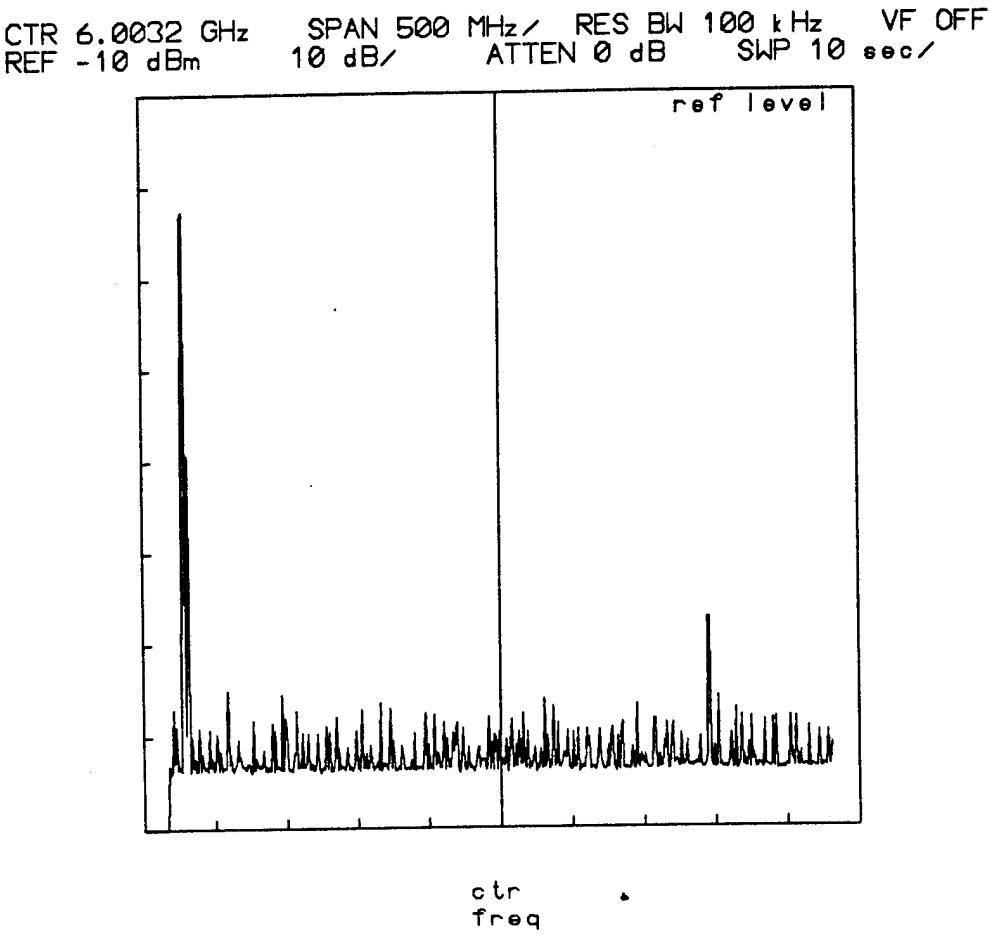

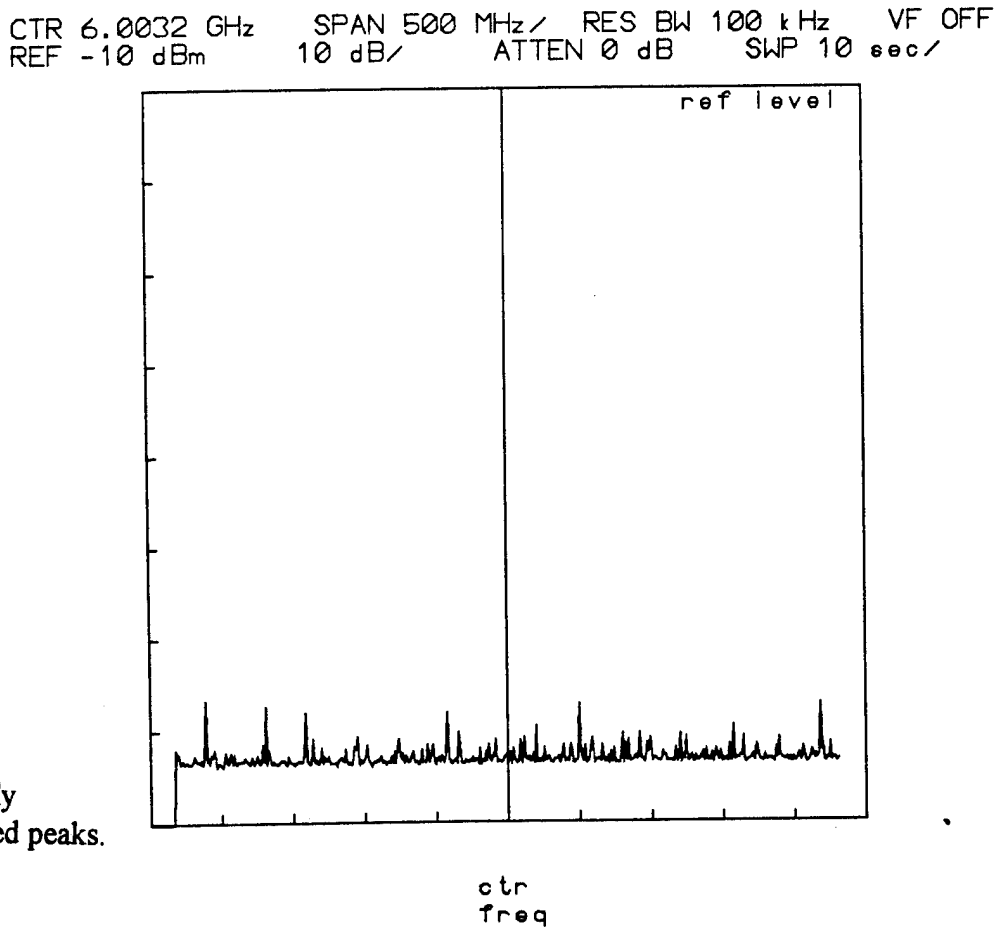

Figure 4
The experimantally observed up shifted peaks.

$$\cos(\beta L) = \cos(k_0 \eta d)\cos[k_0(d-L)] + (1/2)(\eta + 1/\eta)\sin(k_0 \eta d)\sin[k_0(d-L)] \quad (2),$$

where $\eta = (1-\omega_p^2/\omega^2)^{1/2}$ the effective dielectric constant of the plasma regions, and β is the propagation constant for the periodic plasma. Shown in Fig. 5 is an example of the band diagram. An examination of the regions where β is real gives the regions where we would expect to find shifted peaks. Fig 5 indicates that a number of small pass bands appear in the region $\omega < \omega_p$, consistent with the experimental observations (Fig. 4).

This estimate of the output spectrum can be confirmed using a finite difference time domain method to solve the wave equation:

$$\frac{\partial^2 E(z,t)}{\partial z^2} - \frac{1}{c^2}\frac{\partial^2 E(z,t)}{\partial t^2} - \frac{\omega_p^2(z,t)}{c^2}E(z,t) = 0 \quad (3).$$

where ω_p is a function of time with a periodic spatial profile. After solving for the time evolution of the field, we apply a Fast Fourier Transform to the time series to obtain the spectrum. These simulations confirm the predictions of the dispersion relation and show:

1. when *d/L* is small many Floquet modes can be excited, with many upshifted peaks, (Fig 6).
2. when ω_p/ω_0 is large we can obtain frequency components greater than $(\omega_0^2+\omega_p^2)^{1/2}$, or downshifted to $\omega < \omega_p$ (Fig. 7).
3. when $d/L \approx 1$ the peak frequencies all approach one another near $(\omega_0^2+\omega_p^2)^{1/2}$.

Thus, the periodic plasma offers many new interesting phenomena over the case of a single slab.

Figure 5

The $\omega - \beta$ dispersion relation (or band diagram) $L = \lambda_0$, $d/L = 0.6$, $\omega_p / \omega_0 = 1.2$

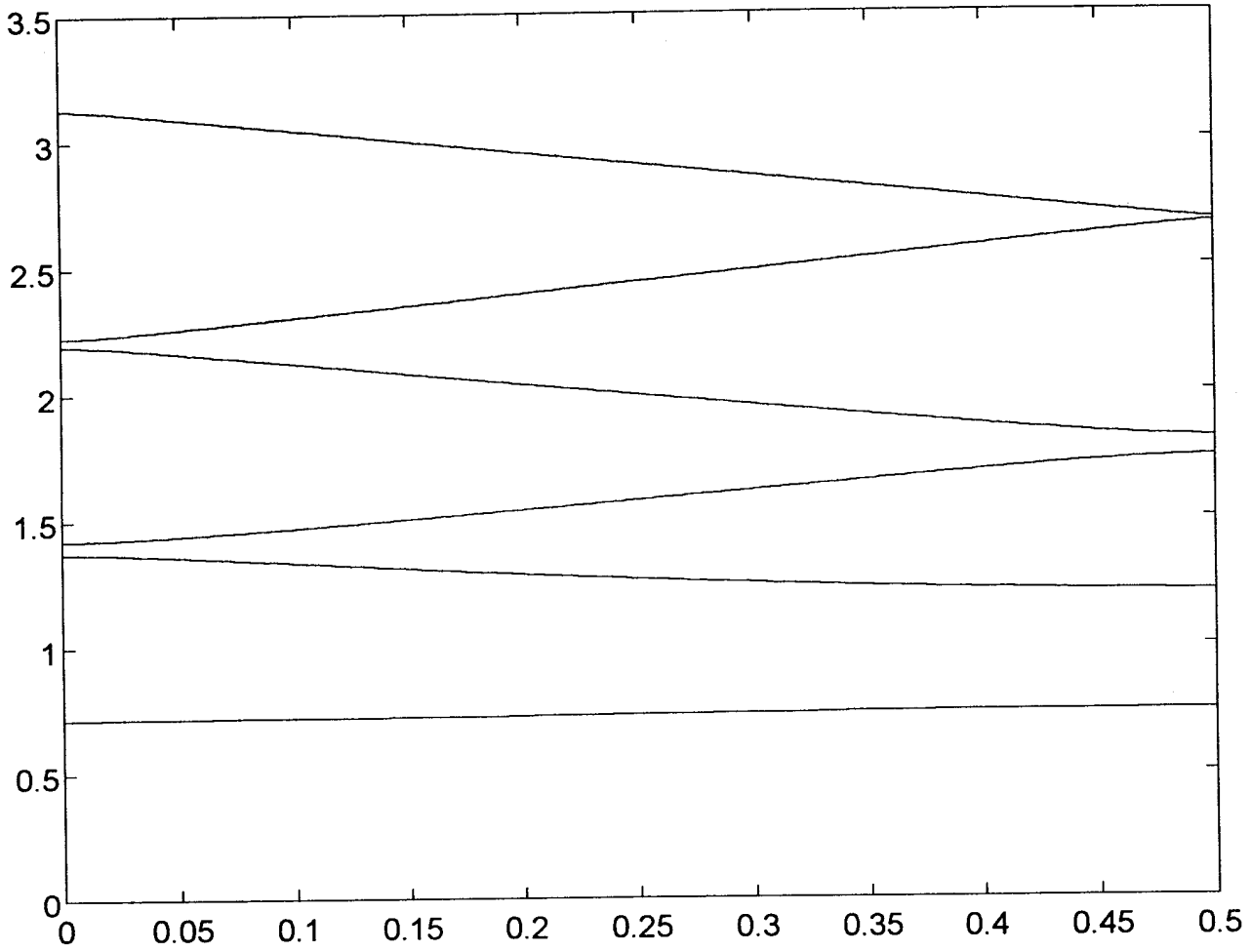

The dispersion curve exhibit a band structure in the frequency range corresponding to an underdense plasma. While in the frequency range corresponding to an overdense plasma (below the plasma frequency), small pass bands emerge.

Figure 6

Frequency Multiplexing

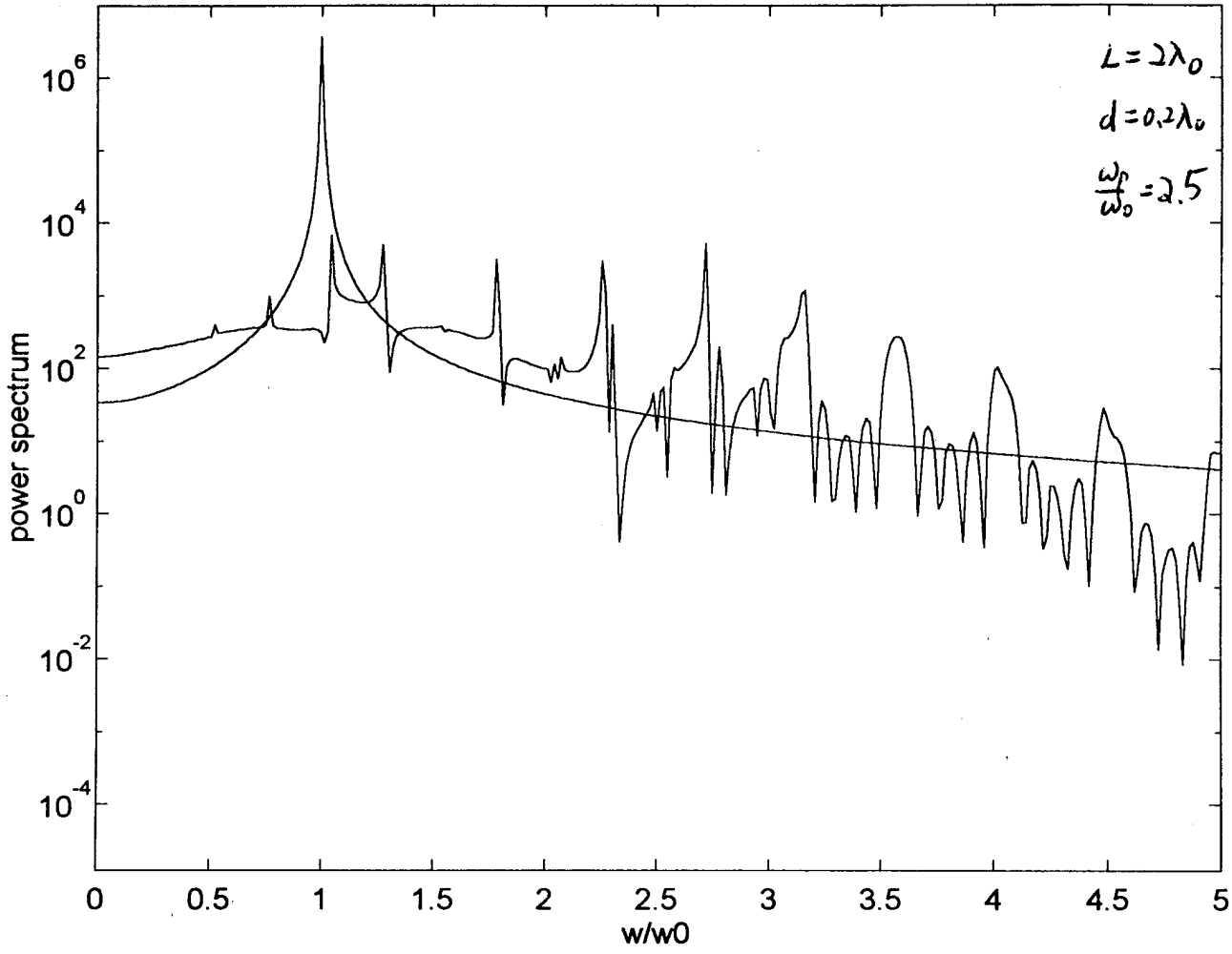

When d / L is small, many Floquet modes can be excited. Moreover, if ω_p / ω_0 is large,, the periodic plasma can effectively shift the initial wave frequency to frequencies larger than $(\omega_0^2 + \omega_{pe}^2)^{1/2}$.

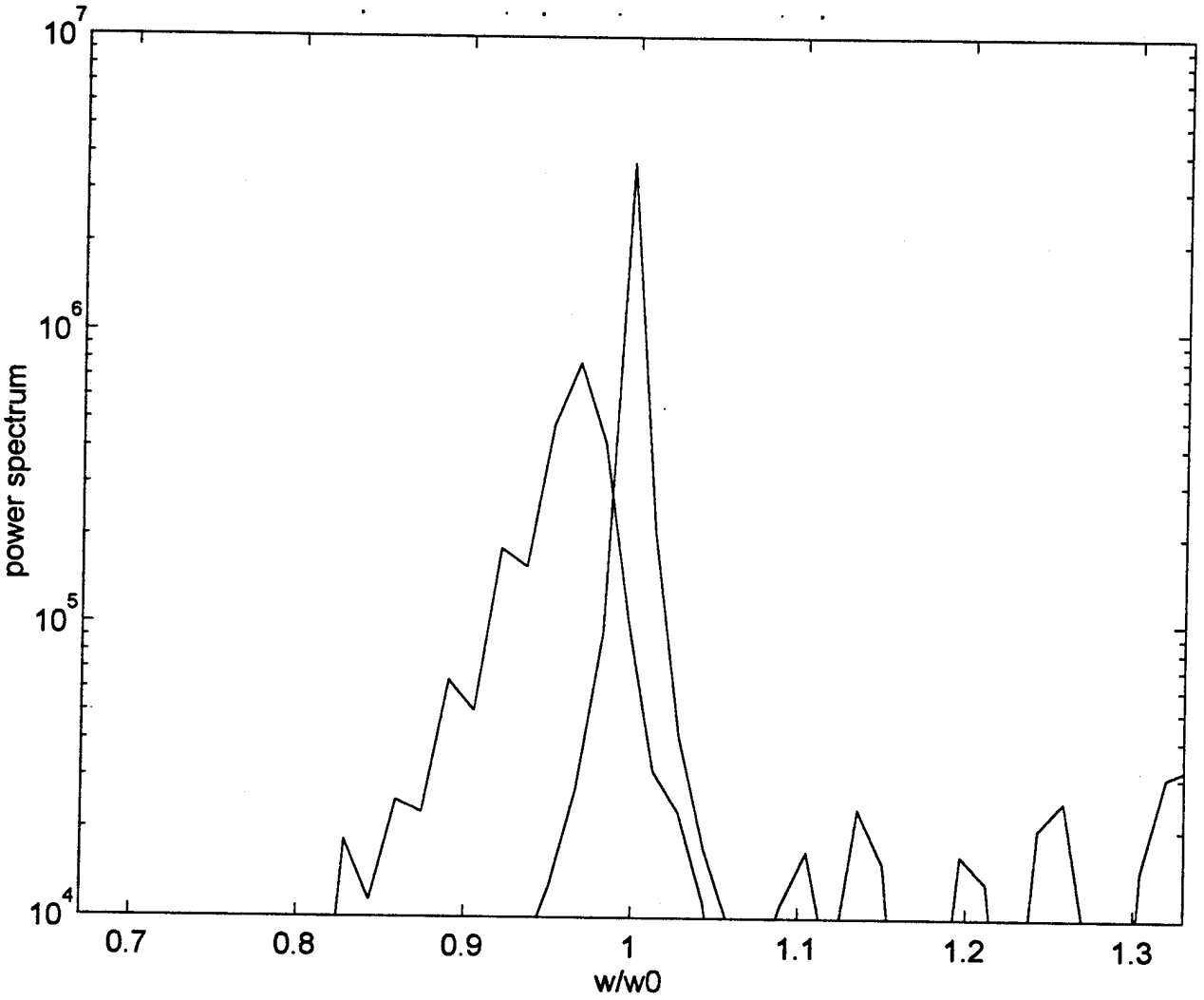

Figure 7

A numerical simulation of the problem, showing similar spectral features to those observed experimentally.

B. Study of Electromagnetic Wave Scattering in Periodically Structured Plasma

Radar cloaking requires a significant attenuation to the backscattered radar signal. There are two approaches to achieve this requirement. One approach is to introduce an absorbing material in front of the target, the other to introduce a structured material instead. The later situation provides for significant side scattering of the incident signal and is believed to be more effective and feasible for the radar cloaking purpose. Therefore, the present work is devoted to the development of a theory describing wave scattering phenomenon in a periodically structured plasma.

The convention scattering theory is based on forward scattering approximations and thus, is limited to small density perturbation. As the density perturbation increases, multiple scattering becomes important. If the perturbation expansion is convergent, the conventional scattering theory can still be applied, but a tedious iteration procedure is involved. Therefore, a quasi-particle theory which includes the multiple scattering process in its formulation is developed. The propagating wave is treated as a group of quasi-particles whose density and momentum distribution are proportional to the spatial and spectral distribution of the wave intensity, respectively. Hence, the distribution of quasi-particles in the phase space can be characterized by a Wigner distribution function which is governed by a "Boltzman" type equation with an effective collision term arising from the quasi-particles interaction with plasma.

This theory is applied for explaining our laboratory experiment, as well as the experimental observations in space plasmas such as: the scintillation of Beacon satellite signals and ionospheric sounding (i.e. spread-F). The work

presented in the following is focused on the study of scintillation phenomena. The scintillation of transionospheric signals is an area of current interest to the Geophysical directory of the Air Force Phillips Laboratory. The conventional theories are not applicable for strong scintillation (i.e. Scintillation index $S_4 > 0.3$). However, many experimental observations conclude that $S_4 > 0.6$ is not unusual in the ionosphere. Therefore, the multiple scattering process must be considered and the innate nature of the quasi-particle theory is particularly suitable for the study of ionospheric scintillation.

The wave characteristics including its amplitude and phase can be described by a joint distribution function of the position vector $\vec{r}$ and the wavevector $\vec{k}$, known as the **Wigner Distribution Function** which is defined to be

$$F(\vec{r},\vec{k},t) = \pi^{-2}\int d\vec{r}' \exp(2i\vec{k}\cdot\vec{r}')\,\psi^*(\vec{r}+\vec{r}',t)\,\psi(\vec{r}-\vec{r}',t) \qquad (1)$$

where ψ is a wave field component and the integration is over all space where the field exists. The quasi-particle spatial density and spectral density can be obtained from the Wigner distribution function by the two relations $|\psi(\vec{r},t)|^2 = \int F(\vec{r},\vec{k},t)d\vec{k}$ and $|G(\vec{k},t)|^2 = \int F(\vec{r},\vec{k},t)d\vec{r}$, respectively.

A single-mode wave equation is considered and expressed as

$$i\frac{\partial\psi}{\partial t} = -(\nabla^2 + {k_o}^2\varepsilon_1(\vec{r}))\psi \qquad (2)$$

The corresponding transport equation of the Wigner distribution function is derived [Ho et al., 1994] to be :

$$\vec{k}\cdot\nabla F = -(k_0{}^2/\pi^2)\int d\vec{k}'F(\vec{r},\vec{k}')\int d\vec{s}\{\varepsilon_{1r}(\vec{r}-\vec{s})\sin[2(\vec{k}-\vec{k}')\cdot\vec{s}] + \varepsilon_{1i}(\vec{r}-\vec{s})\cos[2(\vec{k}-\vec{k}')\cdot\vec{s}]\} \quad (3)$$

where $\varepsilon_1(\vec{r}) = \varepsilon(\vec{r}) - \varepsilon_0 = \varepsilon_{1r}(\vec{r}) + i\varepsilon_{1i}(\vec{r})$ and ε_O is the permittivity of the unperturbed background.

The right hand side of the transport equation (3) can be written

$$\left[(k_o + k_x)\frac{\partial}{\partial x} + k_y\frac{\partial}{\partial y}\right]F = -(k_o{}^2/\pi^2)G_1 \otimes F \quad (4)$$

where

$$G_1(\vec{r},\vec{k}-\vec{k}') = \int d\vec{s}'\{\varepsilon_{1r}(\vec{r}-\vec{s})\sin(2(\vec{k}-\vec{k})\cdot s) + \varepsilon_{1i}(\vec{r}-\vec{s})\cos(2(\vec{k}-\vec{k}')\cdot\vec{s})\}$$

and $\otimes$ stands for convolution.

The first three momentum moments of the quasi-particle distribution function are $\rho = \int d\vec{k}F(\vec{r},\vec{k})$, $\vec{J} = \int d\vec{k}\vec{k}F(\vec{r},\vec{k}) = \vec{k}_0\rho + \vec{J}_1$, and $\underline{\underline{s}} = \int d\vec{k}\vec{k}\vec{k}F(\vec{r},\vec{k}) = \vec{k}_0\vec{k}_0\rho + \vec{k}_0\vec{J}_1 + \vec{J}_1\vec{k}_0 + \underline{\underline{s}}_1$; which are the quasi-particles' number density, current density and stress tensor respectively. The governing moment equations can be derived from (4) and the first two moment equations are found to be

$$k_o\frac{\partial\rho}{\partial x} + \nabla\cdot\vec{J}_1 = -k_o{}^2\rho\varepsilon_{1i}(\vec{r})$$

and (5)

$$k_o \frac{\partial}{\partial x} \bar{J}_1 + \nabla \cdot \underline{\underline{s}}_1 = -k_o{}^2 \bar{J}_1 \varepsilon_{1i}(\vec{r}) + k_o{}^2 \frac{\rho}{2} \nabla \varepsilon_{1r}(\vec{r})$$

We now consider wave scattering within a layer of plasma. The plasma is perturbed by density irregularities represented by a two dimensional spatial variation of the form

$$n(x,y) = P_\ell(x-\ell)\{n_o + \Delta n[1-(\sin k_{11}x - \sin k_{10}x)/\Delta k_1 x\}$$
$$[1-(\sin k_{21}\eta - \sin k_{20}\eta)/\Delta k_2 \eta]\} \quad (6)$$

where $\eta = \cos\theta(y + x\tan\theta)$, $P_\ell(x) = 1$ for $|x| \le \ell$ and 0 for $|x| \ge \ell$ represents a gate function. This density variation can be decomposed into two separate components. The first is characterized by $\langle k_1 \rangle = (k_{11} + k_{10})/2 = 2\pi/d_1$ with the average periodicity d_1 in the longitudinal direction. The second component has an average periodicity d_2, characterized by $\langle k_2 \rangle = (k_{21} + k_{20})/2 = 2\pi/d_2$, oblique to the first with an angle $\phi = \pi/2 - \theta$; n_o is the background plasma density, and Δn is the amplitude of the density irregularity.

This variation consists of two gratings offset from each other by an angle ϕ as illustrated in Fig. 8. As shown these two gratings extend to infinity in the transverse direction and have a finite extent 2ℓ along the downward propagation direction.

It is expected that a model provides a description of irregularities and not resulting signal scintillation exclusively [Fremouw et al., 1984]. This model provides a useful description of BSS irregularities containing

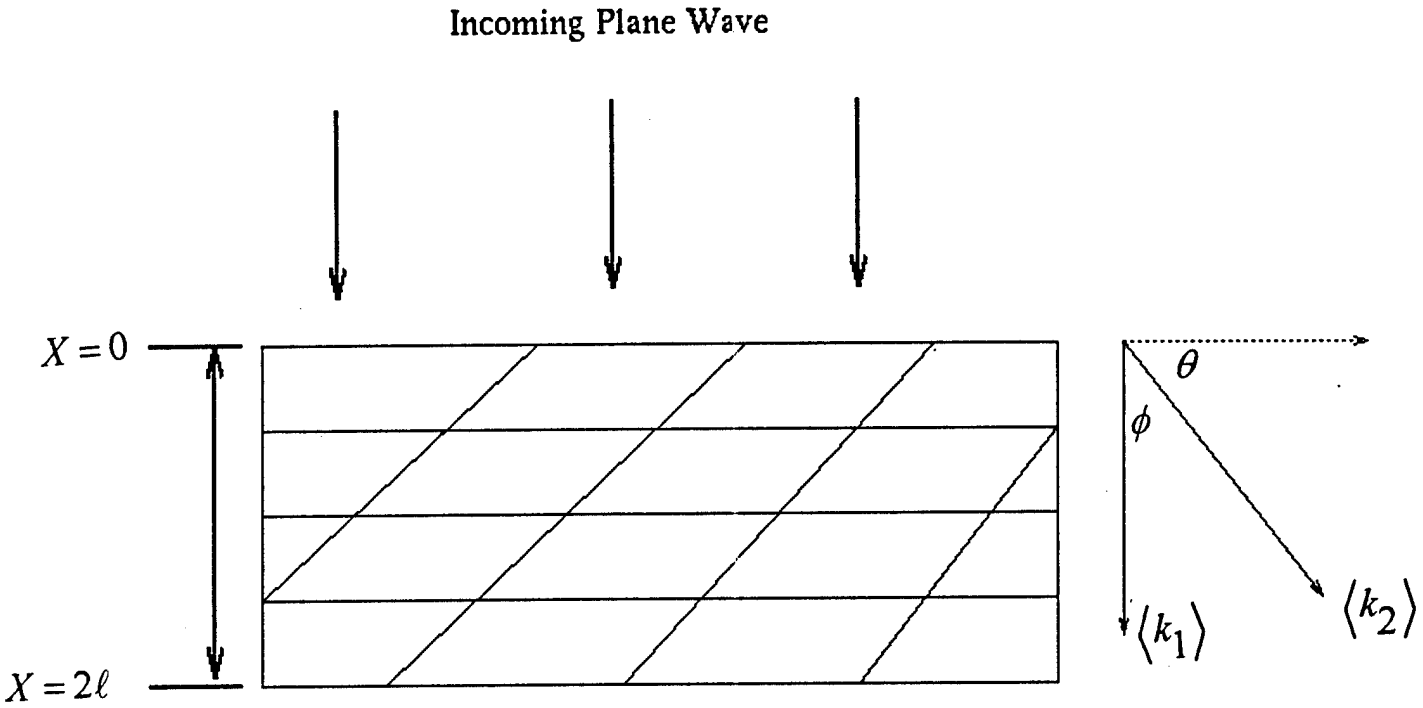

Fig. 8. Incoming plane wave is scattered by a two-dimensional irregularity grating characterized with grating wavevectors $\langle k_1 \rangle$ and $\langle k_2 \rangle$ offset by angle ϕ. The thickness of the irregularity region is 2ℓ.

information on irregularity shape as well as strength. In addition parameterization allows adjustment due to geophysical changes.

The complex dielectric function is derived from the plasma density function as

$$\varepsilon(x,y) = 1 - [\omega_{po}{}^2 / (\omega^2 + \nu^2)](1 - i\nu/\omega) P_\ell(x - \ell)$$
$$\{1 + \beta[1 - \delta_1(x)][1 - \delta_2(\eta)]\}$$

$$= \varepsilon_0 + \varepsilon_1(x,y) \qquad (7)$$

where $\delta_i(\xi) = (\sin k_{i1}\xi - \sin k_{i0}\xi)/\Delta k_i \xi$, $k_{i0} \le k_i \le k_{i1}$, $\Delta k_i = k_{i1} - k_{i0}$ for i=1,2. δ is the Dirac delta function, $\varepsilon_o = 1 - \alpha P_\ell(x - \ell)(1 - i\nu/w)$, $\varepsilon_\ell = -\beta\alpha P_\ell(x - \ell)[1 - \delta_1(x)][1 - \delta_2(\eta)]$, $\omega_p / 2\pi$ is the background electron plasma frequency, ω is the wave angular frequency, ν is the electron-ion collision frequency, $\beta = \Delta n / n_0$ is the percentage of density fluctuation with respect to the background plasma density, and $\alpha = \omega_p^2/(\omega^2 + \nu^2) << 1$ is assumed.

To truncate the hierarchy of the moment equations, a cold quasi-particle distribution is assumed. This assumption is based on the fact that the beacon signal is monochromatic and, hence, the initial quasi-particle distribution has zero temperature. Thus, the second moment tensor $\underline{\underline{s_1}}$ becomes zero and the two moment equations in (5) form a closed set of equations for further analysis. With the aid of (7) the two equations in (5) become

$$k_o \frac{\partial}{\partial x}\rho + \nabla \cdot \vec{J}_1 = \alpha\beta k_o^2 \rho\left(-v/wP_\ell(x-\ell)[1-\delta_1(x)][1-\delta_2(\eta)]\right)$$

and (8)

$$k_o \frac{\partial}{\partial x}\vec{J}_1 + \nabla \cdot \underline{\underline{S}}_1 = \alpha\beta k_o^2 \vec{J}_1\left(-v/wP_\ell(x-\ell)[1-\delta_1(x)][1-\delta_2(\eta)]\right)$$

$$+\alpha\beta k_o^2 \rho\Big\langle\ \hat{x}\frac{\pi}{2}\{[1-\delta_2(\eta)]((\delta(x-2\ell)-\delta(x))[1-\delta_1(x)]$$
$$+P_\ell(x-\ell)[\delta_1(x)/x - k_{11}\cos k_{11}x + k_{10}\cos k_{10}x/\Delta k_1 x])$$
$$+P_\ell(x-\ell)[1-\delta_1(x)](\sin\theta/\eta)(\delta_2(\eta)$$
$$-k_{21}\cos k_{21}x + k_{20}\cos k_{20}x/\Delta k_2])$$
$$+\hat{y}P_\ell(x-\ell)[1-\delta_1(x)](\cos\theta/\eta)(\delta_2(\eta)$$
$$-k_{21}\cos k_{21}x + k_{20}\cos k_{20}x/\Delta k_2])$$

The Scintillation Index is then calculated as:

$$S_4 = \left([<\rho^2> - <\rho>^2]\ /\ <\rho>^2\right)^{1/2},$$

where the average is performed over a spatial period of the transverse irregularity, only the intensity distribution $\rho = |\psi(\vec{r},t)|^2$ of the wave is needed.

The observations showed that the ionosphere irregularities having nearly sinusoidal waveforms in the plasma density extended up to 7000 km in the E-W directions. The rms irregularity amplitude was about 3.5% of the background electron density, which was about $9.9x10^{10}m^{-3}$. The thickness of the irregularity layer was about 35 km. The satellite was located at an altitude of about 400 km and the slant range of the signal was about 600 km. Thus, in the numerical analysis we have chosen $\Delta k_1=0$ and $d_1=2\ell$, β=3.5%,

n_o=9.9 x $10^{10}m^{-3}$, 2ℓ=50km, and 350km for the free space propagation from the bottom of the layer to the ground.

The calculations include the effect of the finite uniform spectral width $\Delta k_2/\langle k_2\rangle$ of the density irregularities on the scintillation index S_4 measured on the ground. The signal frequencies considered are 250MHz and 1541MHz. The optimized S_4 is evaluated, for each frequency by choosing $d_2 = (2\lambda L)^{1/2}$ so that L=350km is the Fresnel size of the signal propagating down from the exit plane of the irregularity region to the ground; where λ is the signal wavelength.

Presented in Fig. 9 is the optimized S_4 for 250MHz beacon signal with d_2= 707 m, an additional case d_2= 1000 m is also shown. The dependence of the optimum S_4 on spectral width $\Delta k_2/\langle k_2\rangle$ is evaluated. It is shown that the location and value of the first peak of the S_4 curve does not varies with d_2 and the peaks are located at zero spectral width. A small spectral width in the irregularity spectrum reduces the optimized S_4 value, the tendency of the effect of spectral width is to reduce the S_4 value. It shows that in the optimized case S_4 drops to a minima near $\Delta k_2/\langle k_2\rangle \approx 0.08$. As $\Delta k_2/\langle k_2\rangle$ increases further above 0.08, the optimized S_4 curve features damped oscillation. Since the values of S_4 in the region of $\Delta k_2/\langle k_2\rangle > 0.08$ are quite small, $\Delta k_2/\langle k_2\rangle < 0.08$ will be the region of interest. The diminishing effect of the spectral width on the S_4 value suggests that the spectral distribution of the irregularities have smeared out the result of the multiple scattering and hence reduced the net scintillation effect on the transverse signals. Similar functional dependences of S_4 for a 1541MHz signal, corresponding to that used by the geostationary beacon satellite Fleetsatcom [Basu et al., 1987], are presented in Fig. 10 showing similar features .The results of Fig. 10 suggest

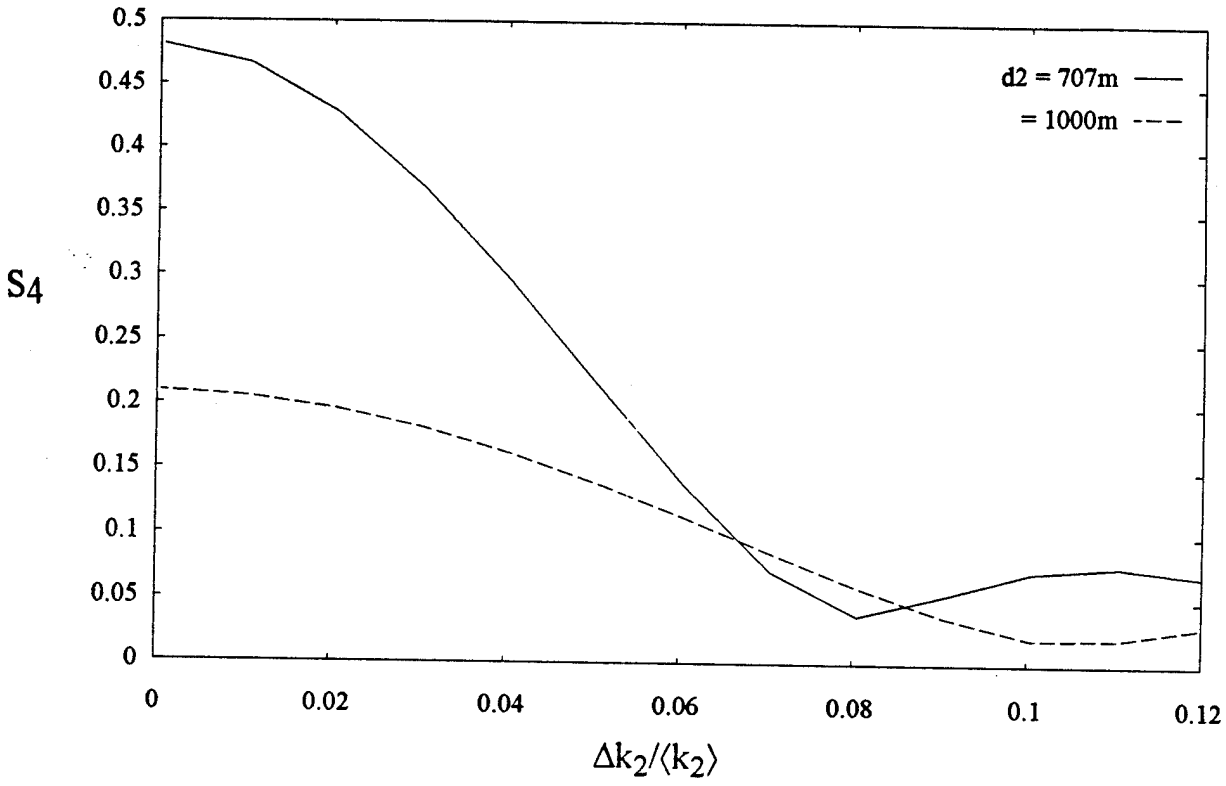

Fig. 9. Dependence of S_4 on spectral width $\Delta k_2/\langle k_2\rangle$ for 250MHz beacon signal, with d_1=50km, d_2= 707 m, 1000 m, 2ℓ=50 km, $n_o = 1\times10^{11} m^{-3}$, ϕ=45°, and β = 3.5%, where d_2=707 m corresponds to optimized S_4.

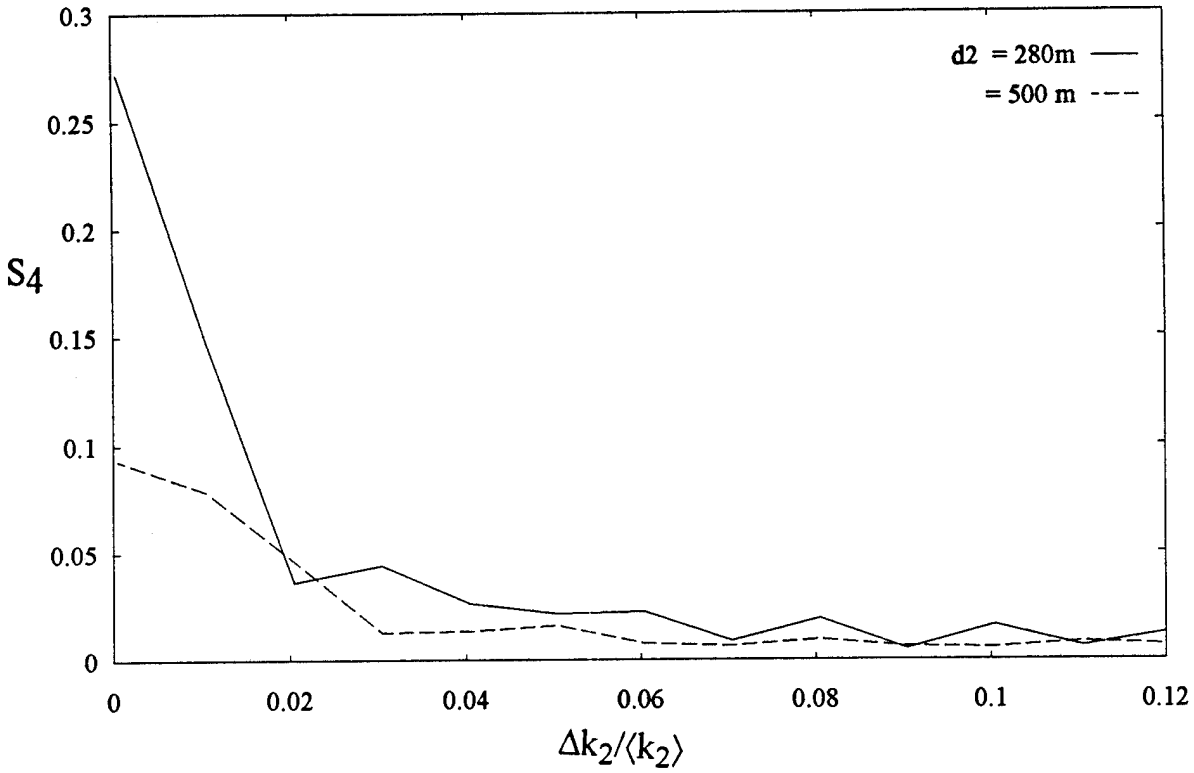

Fig. 10. Dependence of S_4 on spectral width $\Delta k_2/\langle k_2\rangle$ for 1541MHz beacon signal, with d_1=50km, d_2= 280 m, 500 m, 2ℓ=50 km, $n_o = 1\times10^{11} m^{-3}$, ϕ=45°, and β = 3.5%, where d_2=280 m corresponds to optimized S_4.

that S_4 decreases as frequency increases which is consistent with common understanding. In addition, it is shown that the minima location of S_4 varies with the frequency as show in Figs. 9 & 10. The first minimum of the optimized S_4 is located at $\Delta k_2/\langle k_2\rangle \cong$ 0.08, .02, for the 250MHz and 1541MHz cases respectfully. The separation of the locations of the S_4 minima for different beacon signal frequencies could be useful for distinguishing the mechanism, (irregularity amplitude or large spectralwidth), responsible for small S_4 values.

The results of Fig. 10 suggest that S_4 decreases as frequency increases which is consistent with common understanding. In addition, it is shown that the minima location of S_4 varies with the frequency as show in Figs. 9 & 10. The first minimum of the optimized S_4 is located at $\Delta k_2/\langle k_2\rangle \cong$ 0.08, .02, for the 250MHz and 1541MHz cases respectfully. The separation of the locations of the S_4 minima for different beacon signal frequencies could be useful for distinguishing the mechanism, (irregularity amplitude or large spectral width), responsible for small S_4 values.

Appendix: Paper submitted to the JGR

Electron Precipitation Caused by Chaotic Motion in the Magnetosphere due to Large Amplitude Whistler Waves

James Faith, S.P. Kuo, and Joe Huang
Weber Research Institute
Polytechnic University
Route 110, Farmingdale, NY 11735

ABSTRACT

In the magnetosphere energetic charged electrons in the radiation belts are trapped by Earth's magnetic field. In the equatorial region where a symmetric mirror field may be assumed, the electrons undergo bounce motion along the lines of force. When a large amplitude whistler wave is present, the motion of the electrons becomes perturbed. The nonlinear interaction due to the spatial dependence of the field quantities causes the motion of some of the trapped particles to become chaotic. This chaotic behavior serves to enhance the electrons' axial kinetic energy, scattering some electrons into the magnetic mirror's loss cone. Thus we offer a possible explanation of the observed electron precipitation in the polar regions.

Introducing a canonical transformation, the Hamiltonian of a trapped electron becomes time independent. With the aid of additional constants of motion, we reduce the equations of motion so that the electron trajectories lie in a three dimensional phase space. We then use a Surface of Section technique to examine the chaoticity of the system. Lyapanov exponent analysis is also used to extend our results to the case of very small bounce frequency, as one would expect in the magnetosphere. Pitch angle scattering techniques are also effective in describing the system with small bounce frequency, and confirm the enhancement of the electron axial kinetic energy.

INTRODUCTION

In the magnetosphere, charged particles (electrons and hydrogen ions) are trapped by the Earth's magnetic field. When these particles are undisturbed they undergo bounce motion about the geomagnetic equator. However, if a large amplitude plasma wave is present in the magnetosphere, particle trajectories may become significantly perturbed. This allows some particles to be scattered into the mirror loss cone, and precipitate into the polar regions along the geomagnetic field lines where they have been observed experimentally.

In the case of electrons, the original experimental evidence for the precipitation was in the observation of "Trimpi events", named for their discoverer [*Helliwell, et. al.*, 1973]. These events are the perturbations of amplitude and/or phase of VLF and LF beacon signals which are trapped in the Earth ionosphere waveguide and are used primarily for navigation purposes. An event is characterized by a rapid onset (~1 s) of the perturbation in the detected signal and a slow recovery (~100 s) back to the original conditions. These perturbations are related to secondary ionization in the ionospheric D region caused by energetic electrons precipitating from the magnetosphere [*Chang and Inan*, 1983]. These secondary ionizations alter the local plasma density, and thus the dielectric constant of the Earth ionosphere waveguide. This, in turn, accounts for the variation in the beacon signal's received amplitude or phase, as the onset of these precipitation events is rapid but the return to the quiescent state is determined by the longer atmospheric recovery time. More recent experiments have given direct confirmation of the presence of energetic electron precipitation [*Arnoldy and Kinter*, 1989]. In these experiments, electron spectrometers have been carried aloft either in satellites, high altitude balloons, or atop rockets.

Common to all methods of observing the electron precipitation is the one to one correspondence of the presence of magnetospheric whistler waves with the precipitation event [*Chang and Inan*, 1985]. Whistler waves have been observed propagating between the Northern and Southern hemispheres along magnetic field lines. These waves can be coupled into the magnetosphere either from natural sources, such as lightning [*Chang*, 1985], or man made ones, such as high power VLF waves transmitted for ionosphere modification experiments [*Wright*, 1975]. In the case of lightning, the sudden current impulse produces radiation throughout the VLF range. These waves are normally trapped by the Earth ionosphere waveguide. However, the presence of numerous "ducts", or field

aligned ionization density irregularities can trap electromagnetic radiation and guide it between hemispheres [*Carpenter and Sulic*, 1988]. The existence of these ducts is confirmed by the ground based observation of whistlers which do not undergo total reflection upon reaching the ionosphere-magnetosphere boundary [*Helliwell*, 1965].

Due to the correlation of the presence of magnetospheric whistler waves and the electron precipitation events, there has been much theoretical work on the interaction of the waves and the trapped radiation belt electrons. All of the previous work has focused on the interaction of waves whose frequency matches that of the electrons' Doppler shifted cyclotron resonance frequency [*Kennel and Petschek*, 1966, *Inan*, 1987, *Villalón and Burke*, 1991], $\omega - \vec{k} \cdot \vec{v} = \Omega_e / \gamma$, where $\gamma = (1 - v^2 / c^2)^{-1/2}$ is the relativistic factor. While this theory has been successful in explaining some of the events, there is experimental evidence that other processes are also important [*Goldberg, et. al.*, 1987].

Additional evidence that this theory may require augmentation derives from the simultaneous observation of precipitation events at geomagnetically conjugate regions in both hemispheres due to a single lightning flash [*Burgess and Inan*, 1990]. In order to match the resonance condition, particles must move in the opposite direction as the wave, since the wave frequency ω is smaller than the electron cyclotron frequency Ω_e for the whistler wave. Thus this process would first precipitate electrons back to the launching point of the wave. In order induce precipitation into the opposite hemisphere, either the electrons themselves must be reflected by the magnetosphere-ionosphere boundary and bounce back to the opposite hemisphere, or the whistler wave must be reflected at the boundary and interact with particles moving in the other direction on its return path. In either event, there would be an appreciable delay between precipitation events in opposite hemispheres, due to the time required for the particles or wave to bounce from one hemisphere to the other. Thus we would like to propose an alternate theory for the electron precipitation that does not favor one direction of precipitation over the other, and therefore is consistent with the simultaneous observation of precipitation events in both hemispheres. Shown in Fig. 1 is an overview of the situation considered.

Previous work has studied the nonlinear interaction between the magnetospheric protons and the axial component of the kinetic Alfvén wave (KAW) fields with applications to particle precipitation [*Prakash*, 1989]. It was found that a large amplitude KAW will induce chaos in a test particle's orbit . Further studies [*Ho, et. al.*, 1994] found

that the inclusion of the transverse components of the wave fields not only lowers the wave amplitude threshold for the onset of chaos, but the chaos also enhances the particle's transverse (radial) displacement, allowing the precipitation of some particles into the equatorial region [*Guzik, et. al.*, 1989], in addition to the loss cone. Confirming evidence for these theories has also been provided by a recent chamber experiment [*Warren and Mauel*, 1995]. Since chaos is believed to be important to the magnetospheric phenomena, and whistler wave-electron interactions cause the precipitation events, we continue our work [*Faith, et. al.*, 1995] on the dynamics of a single trapped electron subjected to a large amplitude whistler wave.

FORMULATION

To simplify the formulation while retaining all the essential physics the magnetic dipole field is replaced by a parabolic scalar potential, $\varphi \propto z^2$, superimposed over a uniform magnetic field, $\vec{B} = B_0\hat{z}$. The parabolic potential, characterized by a bounce frequency ω_b, simulates the mirror effect of the dipole field. Justification for this simplification is as follows:

A parabolic mirror field in cylindrical coordinates may be describes as:

$$\vec{B} = B_0\left[1+(z^2-r^2)/L^2\right]\hat{z} - B_0 z\hat{r}/L^2,$$

where L is the scale length of the magnetic field. One can show that this magnetic field profile satisfies both $\nabla\cdot\vec{B}=0$ and $\nabla\times\vec{B}=0$, as one would expect in the magnetosphere. The z component of the equation of motion of an electron in the above field is given by:

$$\frac{d}{dt}v_z = \frac{d^2}{dt^2}z = -\frac{e}{m}B_0 z r v_\theta / L^2 = -\frac{\mu B_0}{mL^2}z = -\omega_b^2 z,$$

where $\mu = erv_\theta/2$ is the magnetic dipole of the electron, and $\omega_b = (\mu B_0 mL^2)^{1/2}$ is the bounce frequency. Thus a parabolic potential may be used to simulate the mirroring effect of the magnetic dipole field. The simplification $\omega_b = const.$ is proper as long as the magnetic moment varies slowly in time. It is also noted that the approximation $\vec{B} = B_0\hat{z}$ applies only when $z^2/L^2 << 1$ and $r^2/L^2 << 1$.

The whistler wave field may be described by the vector potential:

$$\vec{A}_w = (B/k)\left[\hat{x}\cos(kz-\omega t) + \hat{y}\sin(kz-\omega t)\right]. \qquad (1)$$

The total vector potential has contributions from both the wave and static fields, and is given by $\vec{A} = \vec{A}_w + \hat{y}B_0 x$. The required scalar potential is given by $\varphi = -(1/2e)m\omega_b^2 z^2$. With both of the potentials given we can derive the classical electron Hamiltonian as:

$$H = (1/2m)\left(\vec{p} + e\vec{A}\right)^2 - e\varphi$$

$$= \frac{1}{2m}\left(p_x^2 + p_y^2 + p_z^2\right) + \frac{m}{2}\left(\frac{\Omega_1}{k}\right)^2 + \frac{m}{2}\omega_b^2 z^2 + \frac{m}{2}\Omega^2 x^2$$

$$+\left(\frac{\Omega_1}{k}\right)\left[p_x \cos(kz - \omega t) - m\Omega x \sin(kz - \omega t)\right] + p_y\left[\Omega x - \frac{\Omega_1}{k}\sin(kz - \omega t)\right] \quad (2)$$

where $\Omega = eB_0/m$, and $\Omega_1 = eB/m$ are the electron cyclotron frequency and a frequency proportional to the wave magnetic field amplitude, respectively.

The equations of motion corresponding to the above Hamiltonian will give trajectories in a six dimensional (plus time) phase space. With a phase space of this many dimensions it is difficult to present results that have clear physical meaning. We therefore seek to simplify the Hamiltonian in a number of ways. First, since energy (equal to the Hamiltonian) is defined only to within an additive constant, the constant term $(m/2)(\Omega_1/k)^2$ may be neglected without altering the system dynamics, and is dropped. Next, the y coordinate is found to be cyclic, meaning p_y is a constant of motion which can be set to zero without loss of generality. Finally we wish to eliminate the time dependence from the Hamiltonian.

We accomplish this by introducing the generating function:

$$F_1(x, Q, t) = \tfrac{1}{2}m\Omega\left(x^2 + Q^2\right)\cot\omega t - m\Omega x Q \csc\omega t. \quad (3)$$

This function provides a canonical transformation with new canonically conjugate coordinates. The new coordinates (Q, P) are related to the old (x, p_x) through the generating function by:

$$p_x = \frac{\partial F_1}{\partial x}, \quad P = -\frac{\partial F_1}{\partial Q},$$

which gives:

$$P = p_x \cos(\omega t) + m\Omega x \sin(\omega t)$$
$$Q = -(p_x / m\Omega)\sin(\omega t) + x\cos(\omega t). \qquad (4)$$

In addition, we can derive the new time independent Hamiltonian from the old one and the generating function through:

$$K = H + \frac{\partial F_1}{\partial t}$$

$$= \frac{1}{2m}\left(1 - \frac{\omega}{\Omega}\right)\left(P^2 + m^2\Omega^2 Q^2\right) + \frac{1}{2m}\left(p_z^2 + m^2\omega_b^2 z^2\right)$$

$$+ \frac{\Omega_1}{k}\left(P\cos kz - m\Omega Q \sin kz\right) \qquad (5)$$

Using Hamilton's equations of motion:

$$\dot{\vec{r}} = \nabla_p K, \quad \dot{\vec{p}} = -\nabla K,$$

and the normalizations to dimensionless quantities:

$$kQ \to Q, \quad kP/m\omega \to P, \quad kz \to z, \quad kp_z/m\omega \to p_z,$$
$$\Omega/\omega \to \Omega, \quad \Omega_1/\omega \to \Omega_1, \quad \omega t \to t, \quad \text{and} \quad \omega_b/\omega \to \omega_b,$$

we can derive the final set of autonomous equations of motion to be integrated numerically:

$$\dot{Q} = \left[(\Omega - 1)/\Omega\right]P + \Omega_1 \cos z$$
$$\dot{P} = -\Omega(\Omega - 1)Q + \Omega\Omega_1 \sin z$$
$$\dot{z} = p_z$$
$$\dot{p}_z = -\omega_b^2 z + \Omega_1\left(P\sin z + \Omega Q \cos z\right) \qquad (6)$$

Since K is a constant of motion, the set of equations (6) describes trajectories in a three dimensional phase space. Thus a surface of section technique can be used to reduce the three dimensional continuous time system to a two dimensional map, where we can examine the chaoticity of the system graphically. It should be stressed that the bouncing motion introduces the chaotic nature to the system. One can show that if there is no bouncing motion, i.e. $\omega_b = 0$, that an additional constant of motion:

$$\tfrac{1}{2}\left(\Omega^2 Q^2 + P^2\right) - \Omega p_z = const.$$

can be found. This is easily verified with the use of the Poisson Bracket. This constant reduces the system to two autonomous equations. A system of this type can never exhibit chaotic motion, and the trajectory will always have regular behavior in a two dimensional phase space.

NUMERICAL ANALYSIS

In the following analysis, with $\omega_b \neq 0$, we choose to eliminate the variable P with the constant of motion K. We choose $Q = 0$ as the surface of section, allowing us to graphically depict the chaoticity of the system with a portrait of the (z, p_z) phase space. It is noted that for a given K, both P and $\dot{Q}$ are double valued. Hence the surface of section is separated into the $\dot{Q} < 0$ and $\dot{Q} > 0$ cases. However, since the two cases are mirror images of each other we choose only to present the $\dot{Q} < 0$ case.

The plots are made by integrating the equations of motion forward in time using a fifth order Runge Kutta ordinary differential equation solver. When the sign of Q changes from positive to negative between two time steps, the trajectory between these two points is interpolated to the $Q = 0$ plane, and the resulting point recorded. The time integration continues for many (~1000) bounce periods. The several orbits on each of the surface of section plots are computed by beginning multiple time integrations from different initial conditions. These are chosen by maintaining a constant transformed Hamiltonian K, and choosing a sequence of $P=n\Delta$, where n=0,1,2,... is an integer and Δ is a value chosen to give about twelve sets of initial conditions. These values of P are used to solve for the proper p_z (as long as p_z remains real!). We find that the behavior of the system is strongly dependent on two quantities, the value of K and the wave amplitude. As Ω_1 is proportional to the wave amplitude and K equals the initial particle energy, we vary these parameters from small to relatively large values to demonstrate the transition from regular behavior to chaos.

For our analysis, we choose parameters corresponding to conditions in the magnetosphere, with the exception of the bounce frequency which is initially chosen much larger than the physical bounce frequency to allow the use of more modest computation times and data file sizes. The results will then be extended to the range of bounce frequencies one would physically expect. The other parameters are chosen to reflect a typical whistler wave propagating along the L=3 shell, where $\Omega/2\pi$=32 kHz, $\omega/2\pi$=13.7

kHz, and a plasma frequency, $\omega_p/2\pi = (ne^2/\varepsilon_0 m)^{1/2}$=15kHz. The plasma frequency is required to find the wavenumber, k, which is related to ω through the whistler wave dispersion relation $\omega = \Omega_e c^2 k^2/\omega_p^2$. As a starting point we also choose the bounce and wave frequencies equal.

First we choose to fix the particle energy and vary the wave amplitude. K is chosen to be 1, which corresponds to the commonly observed particle energy of 180 keV. With a very small wave amplitude, $\Omega_1 = 0.1$, the trajectories in Fig. 2a are found to be regular for all initial conditions. Increasing the wave field to $\Omega_1 = 0.4$ in Fig. 2b, the trajectories are noticeable distorted by the larger wave, and the entire surface of section is pushed into the $p_z < 0$ portion of phase space. Continuing to increase the wave field to $\Omega_1 = 0.43$ for Fig. 2c the trajectories for several initial conditions become chaotic, as shown by the irregular smear of dots in the upper portion of the plot. Finally, one last increase in the wave amplitude to $\Omega_1 = 0.6$ in Fig. 2d shows all of the regular orbits replaced by chaos throughout the plot.

The second parameter that strongly influences the dynamics of the system is the particle energy. For all the plot in this figure, the cyclotron , wave, and bounce frequencies are all held constant at $\Omega = 2.333$, $\Omega_1 = 0.46$, and $\omega_b = 1.0$. In the first plot, Fig. 3a, the initial particle energy is 45keV, corresponding to K=0.25. The trajectories are regular for all initial conditions. With K=0.5, Fig. 3b, the trajectories all remain regular, although some distortion is seen from the previous case. Once the particle energy is increases to K=0.7, Fig. 3c, the onset of chaos has been observed in the heavy smear of dots in the center of the plot. Finally, a small further increase in K to K=0.75, Fig. 4d, caused the trajectories to become chaotic over the majority of the plot.

To extend the results to a more realistic bounce frequency, $10^{-3} \le \omega_b \le 10^{-2}$, two techniques are available to us. The first involves the use of Lyapanov exponent analysis. These exponents are the rates of exponential separation of two initially close points in phase space. As this exponential separation defines a chaotic system, a positive Lyapanov exponent means the system is chaotic. Presented in Fig. 4 is the dependence of the first two Lyapanov exponents on the bounce frequency. Since in Hamiltonian systems the exponents occur only in oppositely signed pairs, only the positive exponents are presented. The exponents were computed for five bounce periods using the method of *Wolf, et. al.*, [1985]. This time is sufficient for the exponents to settle to their asymptotic values.

The second way to extend our results to the case of small bounce frequencies is to define the pitch angle α as:

$$\alpha = \tan^{-1}(v_\perp / v_\parallel) = \tan^{-1}(\sqrt{v_x^2 + v_y^2} / v_z), \tag{7}$$

where the true velocities are related to the canonical momenta and our transformed and normalized variables as:

$$mv_x = p_x + eA_x = P\cos\omega t - m\Omega Q \sin\omega t + (m\Omega_1 / k)\cos(\omega t - kz)$$
$$\rightarrow P\cos t - \Omega Q \sin t + \Omega_1 \cos(t - z)$$

$$mv_y = p_y + eA_y = P\sin\omega t + m\Omega Q \cos\omega t + (m\Omega_1 / k)\sin(\omega t - kz)$$
$$\rightarrow P\sin t + \Omega Q \cos t + \Omega_1 \sin(t - z)$$

$$mv_z = p_z \rightarrow p_z.$$

The quantity α is especially of interest when the electron is at the geomagnetic equator (z=0), where it can be compared with the loss cone angle. If at this plane the pitch angle is less than the loss cone angle the particle has enough axial momentum to escape out the end of the magnetic mirror field, and precipitate into the polar regions. Shown in Fig. 5 is the equatorial pitch angle plotted against time for four bounce frequencies, $\omega_b = 1.0, 10^{-1}, 10^{-2}, 10^{-3}$, in Figs. 5a, 5b, 5c, and 5d, respectively. In all cases it is found that in the chaotic case the pitch angle varies wildly and for all bounce frequencies achieves lower pitch angles, and can more readily escape.

CONCLUSION

We have shown that the nonlinear interaction arising from the spatial dependence of the fields of a large amplitude whistler wave with a trapped bouncing electron can lead to chaos in the electron trajectory. In addition, we have found that it is the bouncing effect that leads to the chaos, as shown by the existence of an additional constant of motion in the case of zero bounce frequency. However, it should be noted that our model of the geomagnetic field, that is of a parabolic potential superimposed over a uniform magnetic field, is valid only in the region near the geomagnetic equator.

The end result of the chaos induced in the electron trajectory is to enhance its axial kinetic energy, as shown in any of the chaotic surface of section plots in the (z, p_z) phase space. This is apparent because when the electron trajectory is regular, it is confined to lay only upon the closed loops seen in Fig. 2a or Fig. 3a. When the wave amplitude becomes larger, and the trajectories become chaotic, the electron trajectory is no longer confined to a closed loop, and may wander throughout the chaotic regions. Thus an electron with an initially small axial kinetic energy may eventually acquire enough energy to be scattered into the loss cone of the magnetic mirror field. In addition, this increase in axial kinetic energy will alter the pitch angles of the trapped particles, as seen in Fig. 5., and allow scattering into the loss cone.

Once electrons are scattered into the loss cone, they follow the geomagnetic field lines and will precipitate into the ionosphere, where they can be detected by the methods discussed in the introduction (and in the references therein). The dissimilarity of this theory as compared to one based on gyroresonant interaction is the fact that here there is no preferred direction of precipitation. Thus particles are equally likely to be scattered in the direction with or against the wave, it offers a possible explanation of the simultaneous observation of precipitation events in geomagnetically conjugate regions in both the Southern and Northern hemispheres [*Burgess*, 1990]. This leads us to believe that the chaotic scattering discussed here can successfully augment the gyroresonant scattering theories.

Acknowledgment. A portion of this work was completed while one of the authors (SPK) was working at the Air Force Phillips Laboratory, Hanscom AFB, MA, whose hospitality is appreciated. The authors also gratefully acknowledge funding support for this work by the Air Force Office of Scientific Research, Grants AFOSR-F49620-92-J-0349 and -94-0076.

REFERENCES

Arnoldy, R.L. and P.M. Kintner, Rocket observations of the precipitation of electrons by ground VLF transmitters, *J. Geophys. Res., 94*, 6825-6832, 1989.

Burgess, W.C. and U.S. Inan, Simultaneous disturbance of conjugate ionospheric regions in association with individual lightning flashes, *Geophys. Res. Lett., 17*, 259-262, 1990.

Carpenter, D.L. and D.M. Sulic, Ducted whistler propagation outside the plasmapause, *J. Geophys. Res., 93,* 9731-9742, 1988.

Chang, H.C. and U.S. Inan, A theoretical model study of observed correlations between whistler mode waves and energetic electron precipitation events in the magnetosphere, *J. Geophys. Res., 88,* 10053-10058, 1983.

Chang, H.C. and U.S. Inan, Lightning induced electron precipitation from the magnetosphere, *J. Geophys. Res., 90,* 1531-1541, 1985.

Faith, J., S.P. Kuo, J. Huang, Chaotic electron motion driven by whistler waves in the magnetosphere, Accepted for publication in *Comments on Plasma Phys. and Controlled Fusion.*

Goldberg, R.A., S.A. Curtis, and J.R. Barcus, Detailed spectral structure of magnetospheric electron bursts precipitated by lightning, *J. Geophys. Res., 92,* 2505-2513, 1987.

Guzik, T.G., M.A. Miah, J.W. Mitchel, and J.P. Wefel, Low altitude trapped protons at the geomagnetic equator, *J. Geophys. Res., 94,* 145-150, 1989.

Helliwell, R.A., *Whistlers and Related Ionospheric Phenomena,* Stanford University Press, Stanford, CA, 1965.

Helliwell, R.A., J.P. Katsufrakis, and M.L. Trimpi, Whistler induced amplitude perturbation in VLF propagation, *J. Geophys. Res., 78,* 5515, 1973.

Ho, A.Y., S.P. Kuo and G. Schmidt, Chaotic proton motion driven by kinetic Alfven waves in the magnetosphere leading to polar and equatorial proton precipitations, *J. Geophys. Res., 99* , 11087-11093, 1994.

Inan, U.S., Gyroresonant pitch angle scattering by coherent and incoherent whistler wave modes in the magnetosphere, *J. Geophys. Res., 92,* 127-142, 1987.

Kennel, C.F., and H.E. Petschek, Limit on stably trapped particle fluxes, *J. Geophys. Res.*, *71*, 1-28, 1966.

Liu, W.W., Chaos driven by kinetic Alfven waves, *Geophys. Res. Lett.*, *18*, 1611-1614, 1991.

Prakash, Manju, Particle precipitation due to nonlinear wave-particle interactions in the magnetosphere, *J. Geophys. Res.*, *94*, 2497-504, 1989.

Villalón, E., and W.J. Burke, Near-equatorial pitch angle diffusion of energetic electrons by oblique whistler waves, *J. Geophys. Res.*, *96*, 9655-9667, 1991.

Warren, H.P. and M.E. Mauel, Observation of chaotic particle transport induced by drift resonant fluctuations in a magnetic dipole field, *Phys. Rev. Lett.*, *74*, 1351-1354, 1995.

Wolf, A. J.B. Swift, H.L. Sweeney, and J.A. Vastano, Determining Lyapanov exponents from a time series, *Physica D Amsterdam*, *16*, 285-317, 1985.

Wright, J.W., Evidence for precipitation of energetic particles by ionospheric 'heating' transmissions, *J. Geophys. Res.*, *80*, 4383-4386, 1975.

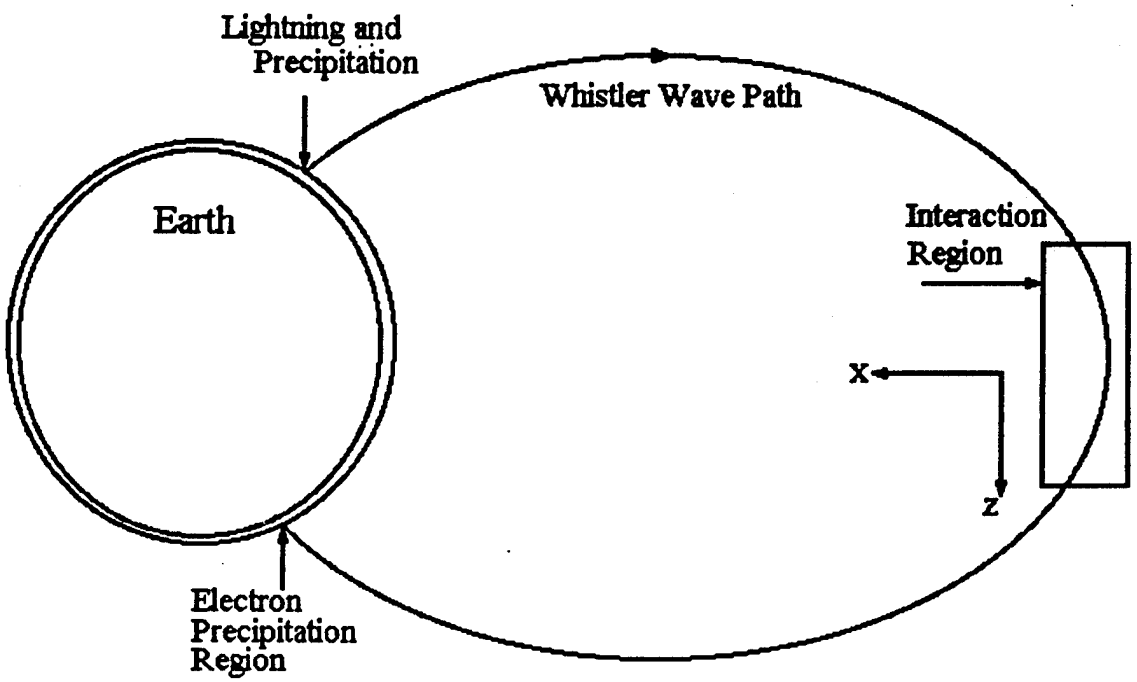

Figure 1.
An overview of the physical situation considered.

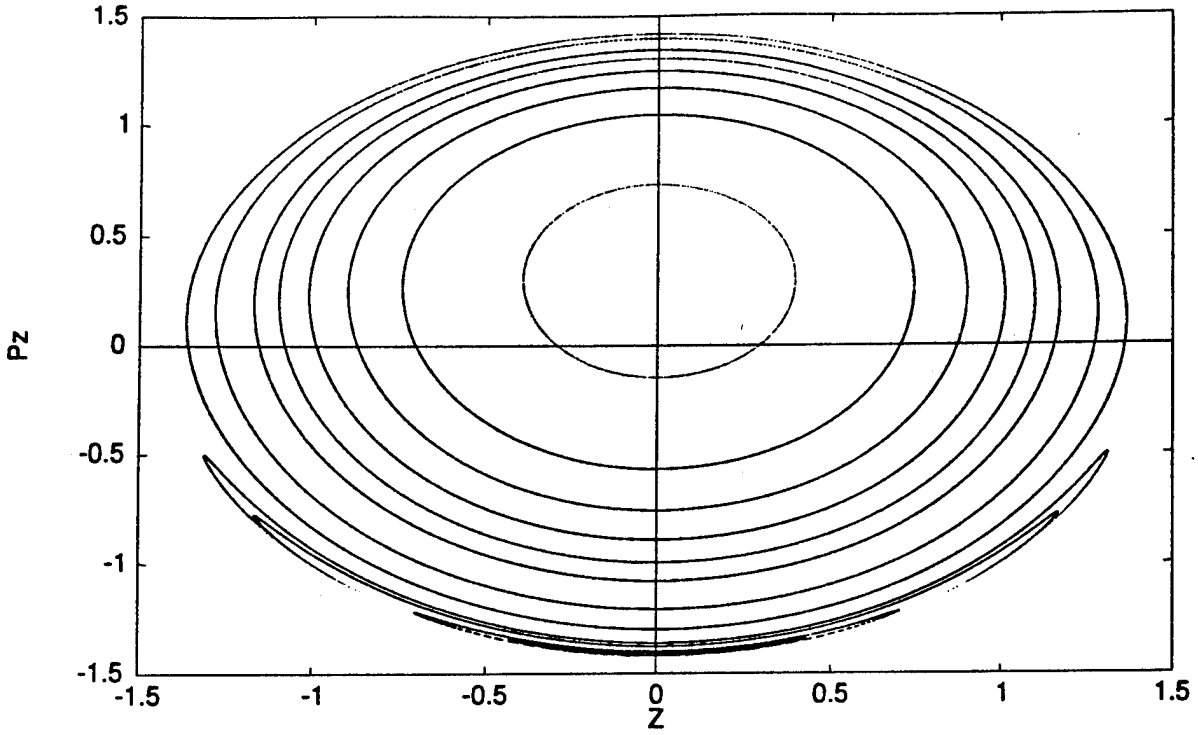

(a)

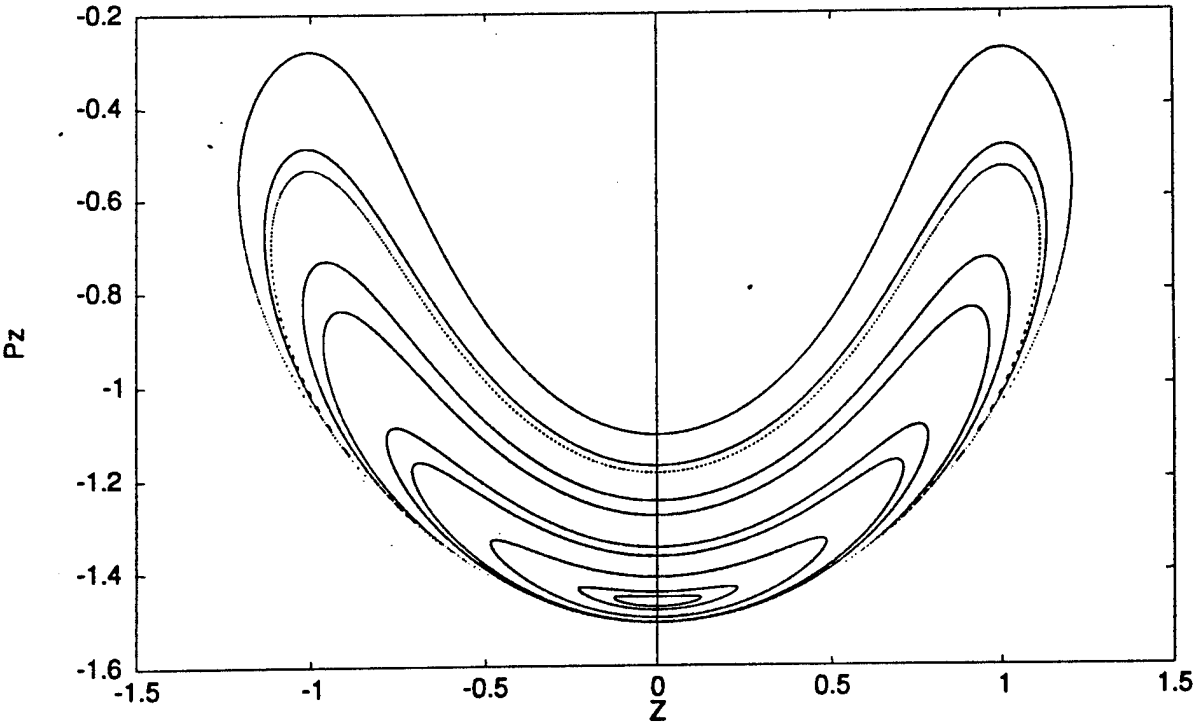

(b)

Figure 2 (a) and (b)

Surface of section plots at the Q=0 plane, with K=1, $\Omega = 2.333$, $\omega_b = 1.0$, and (a) $\Omega_1 = 0.1$, and (b) $\Omega_1 = 0.4$. Both plots show only regular behavior.

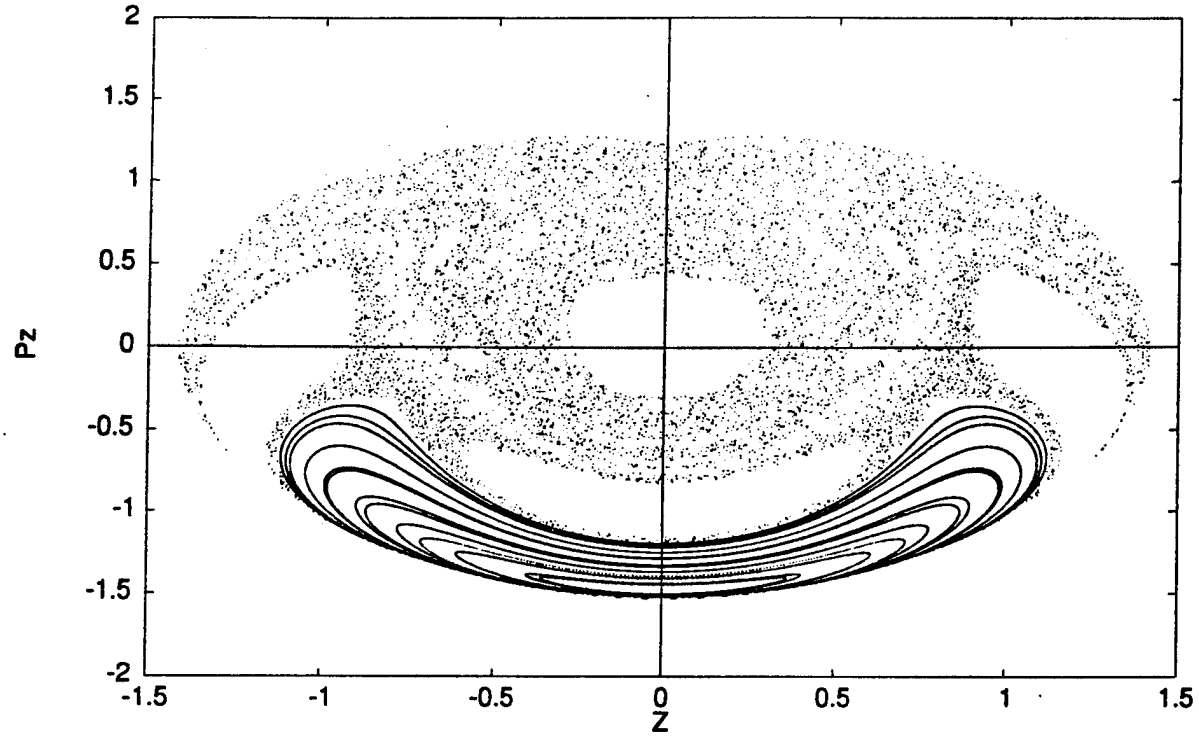

(c)

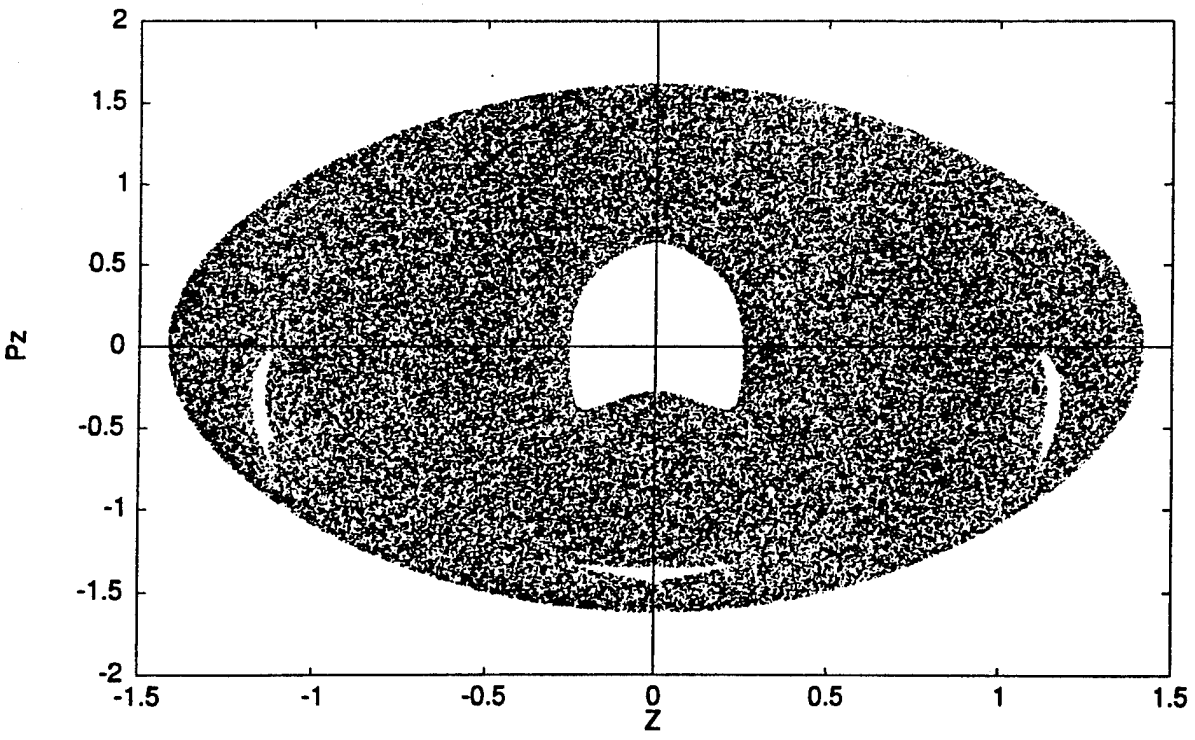

(d)

Figure 2 (c) and (d)

Surface of section plots at the Q=0 plane, with K=1, $\Omega = 2.333$, $\omega_b = 1.0$, and (c) $\Omega_1 = 0.43$ showing both chaotic and regular regions, and (d) $\Omega_1 = 0.6$ showing only chaotic regions.

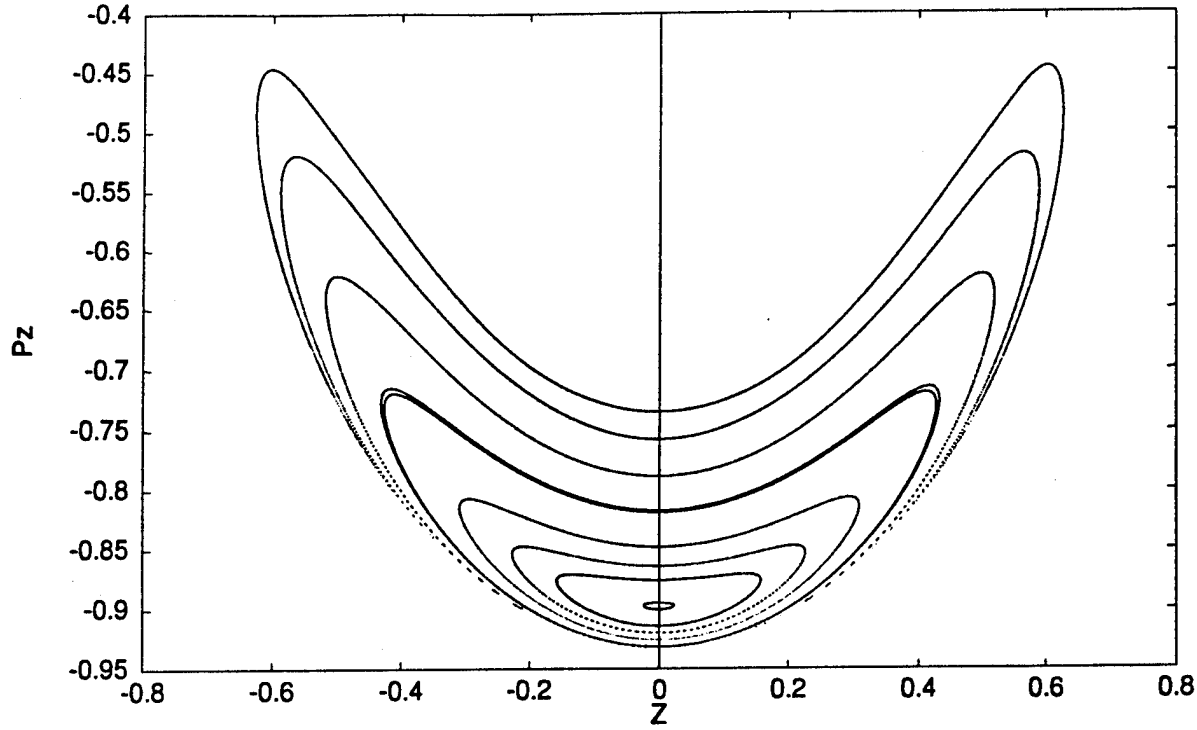

(a)

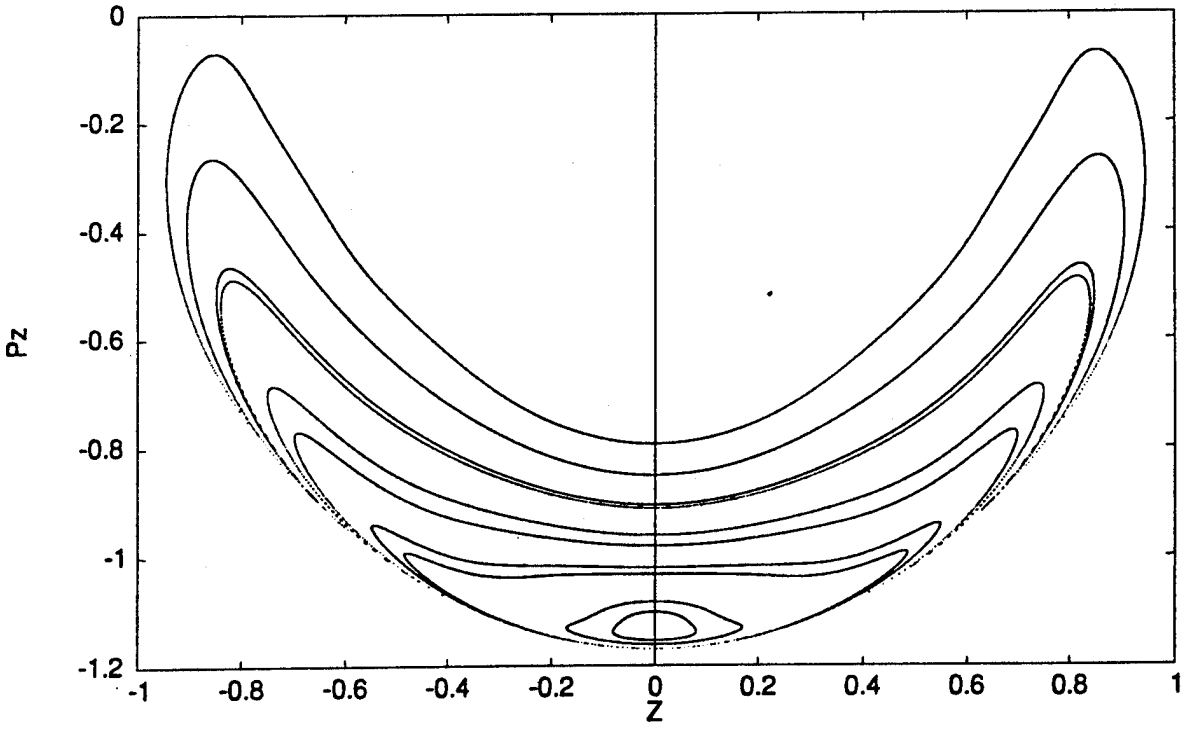

(b)

Figure 3 (a) and (b)

Surface of section plots at the Q=0 plane, with $\Omega = 2.333$, $\Omega_1 = 0.46$, and $\omega_b = 1.0$, and (a) K=0.25, and (b) K=0.5. Both plots show only regular behavior.

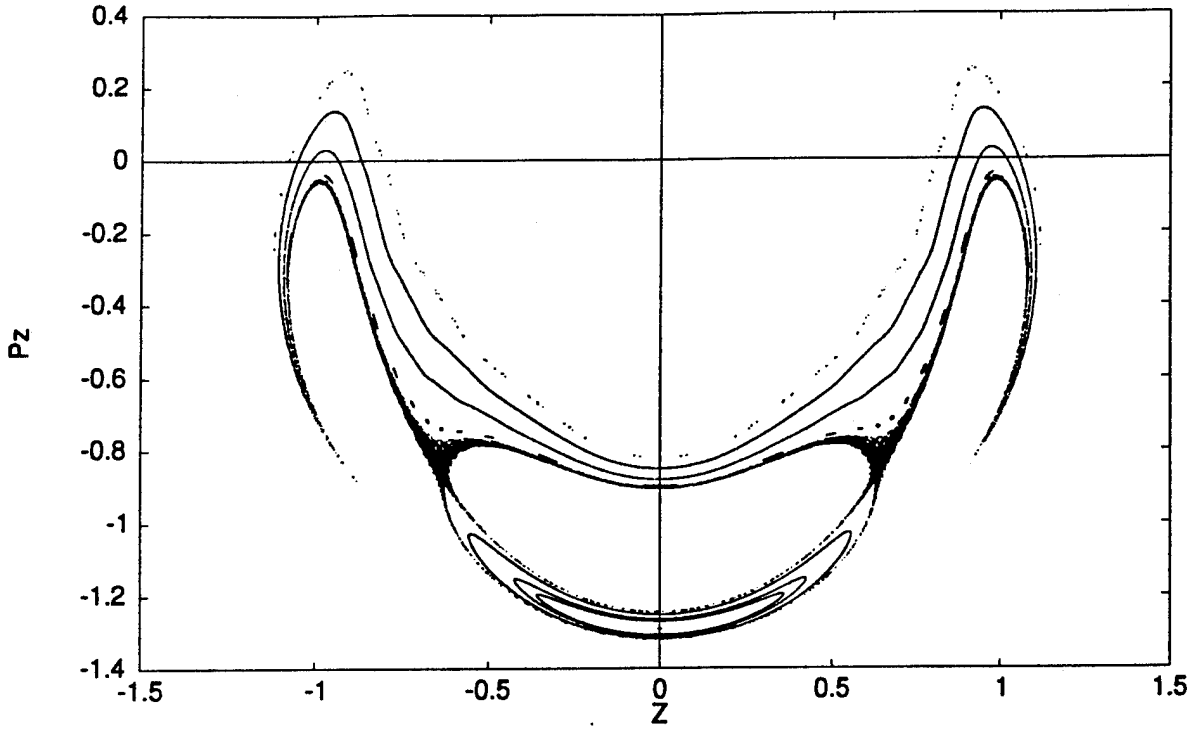

(c)

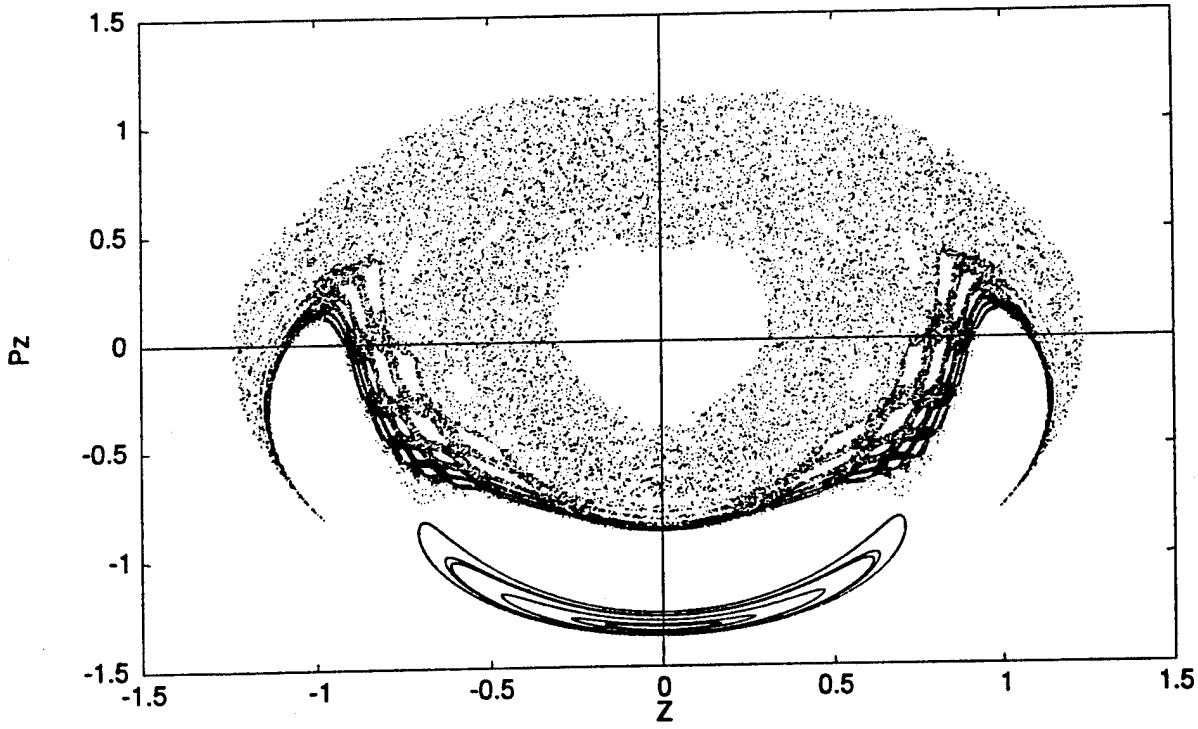

(d)

Figure 3 (c) and (d)

Surface of section plots at the Q=0 plane, with $\Omega = 2.333$, $\Omega_1 = 0.46$, and $\omega_b = 1.0$, and (c) K=0.7, and (d) K=0.75. Both plots show both regular and chaotic behavior.

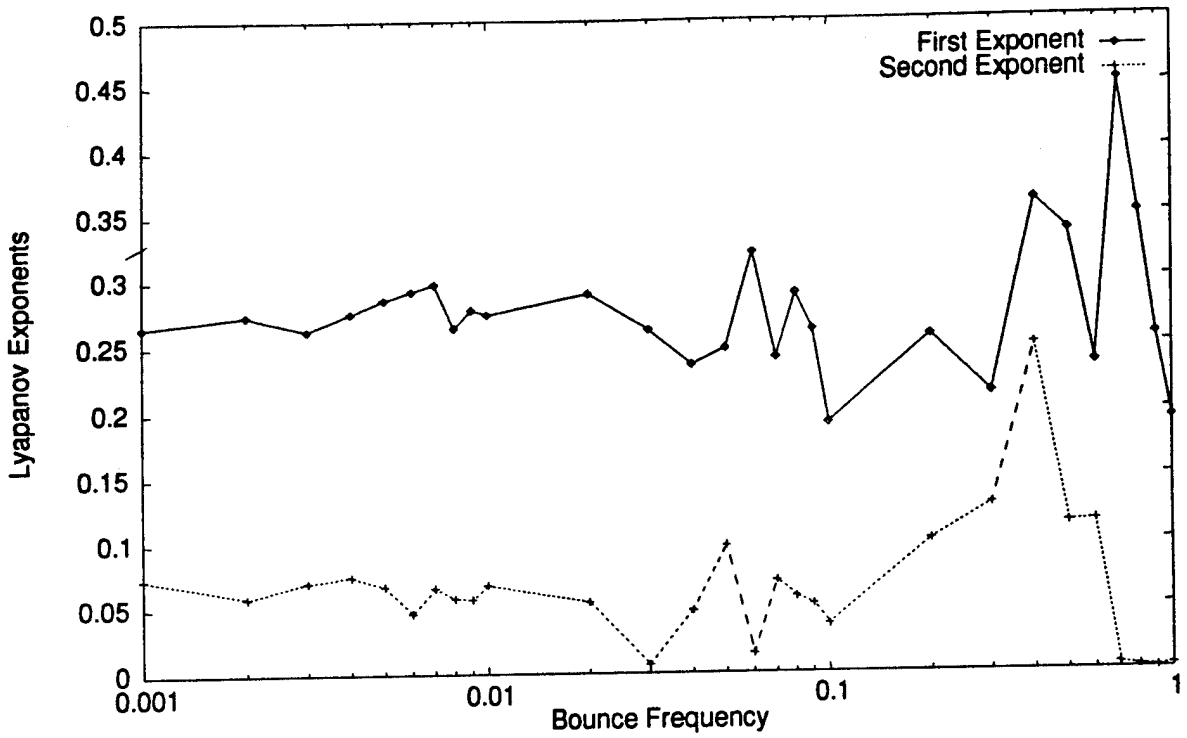

Figure 4

Functional dependence of first two Lyapunov exponents an the bounce frequency, K=1, $\Omega = 2.333$, $\Omega_1 = 0.46$, $Q_0 = z_0 = 0$, $P_0 = 1.2$, $p_{z0} = 0.27$, and $10^{-3} \leq \omega_b \leq 1$. The system is chaotic for all bounce frequencies.

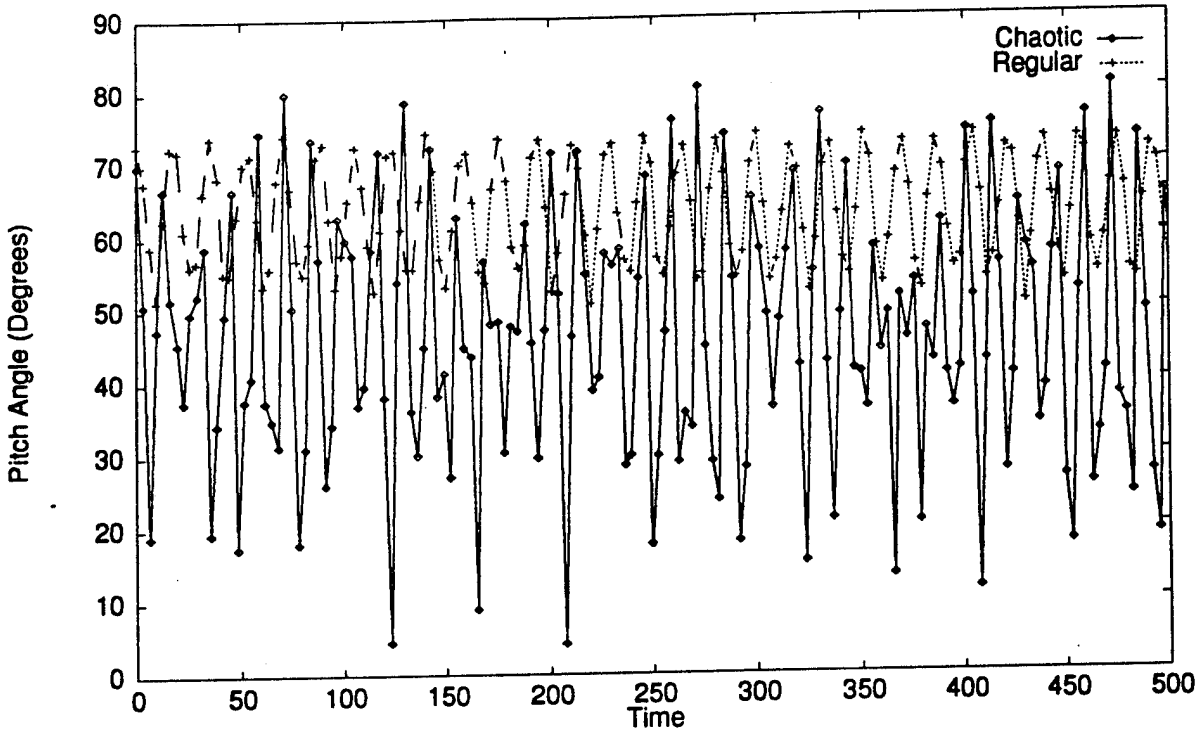

(a)

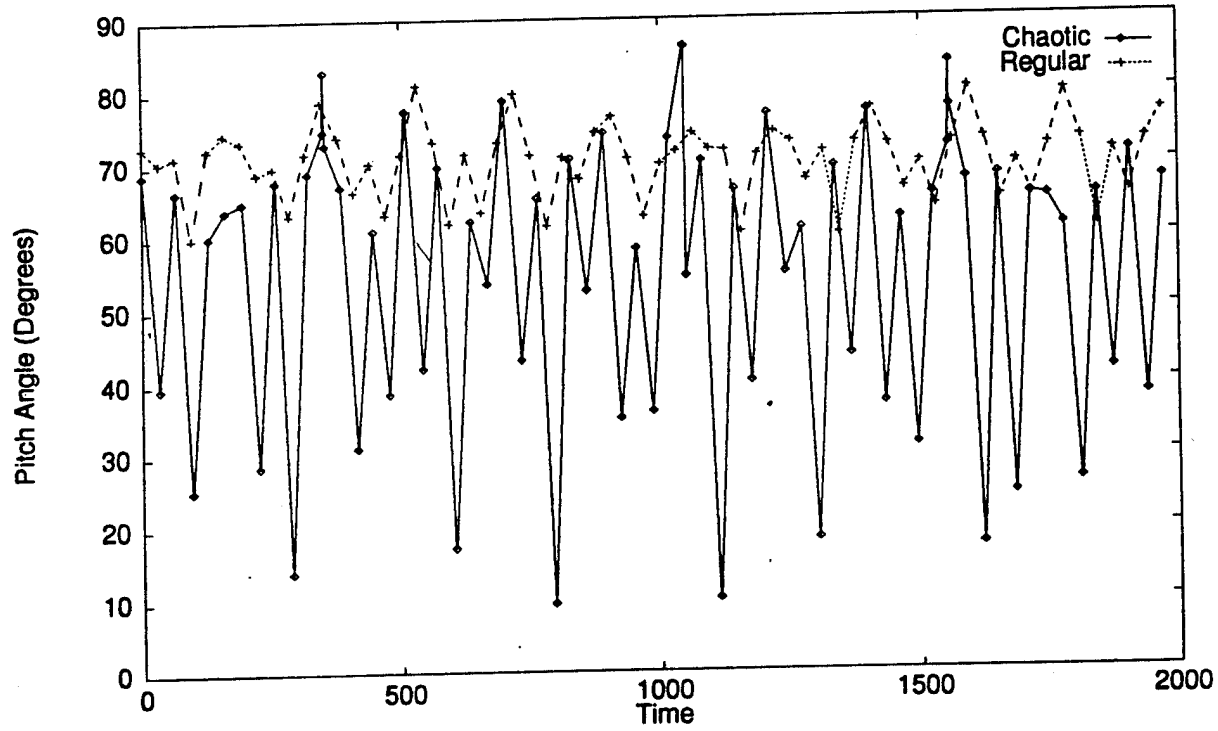

(b)

Figure 5 (a) and (b)

Functional dependence pitch angle at the geomagnetic equator on time for K=1, $\Omega = 2.333$, $Q_0 = z_0 = 0$, $\omega_b = 1.0$ (a), and $\omega_b = 0.1$ (b). The chaotic plot is for $\Omega_1 = 0.46$, $P_0 = 1.6$, and $p_{z0} = 0.46$, while the regular is for $\Omega_1 = 0.1$, $P_0 = 1.2$, and $p_{z0} = 0.27$. Both plots have $\alpha_0 \approx 70^\circ$.

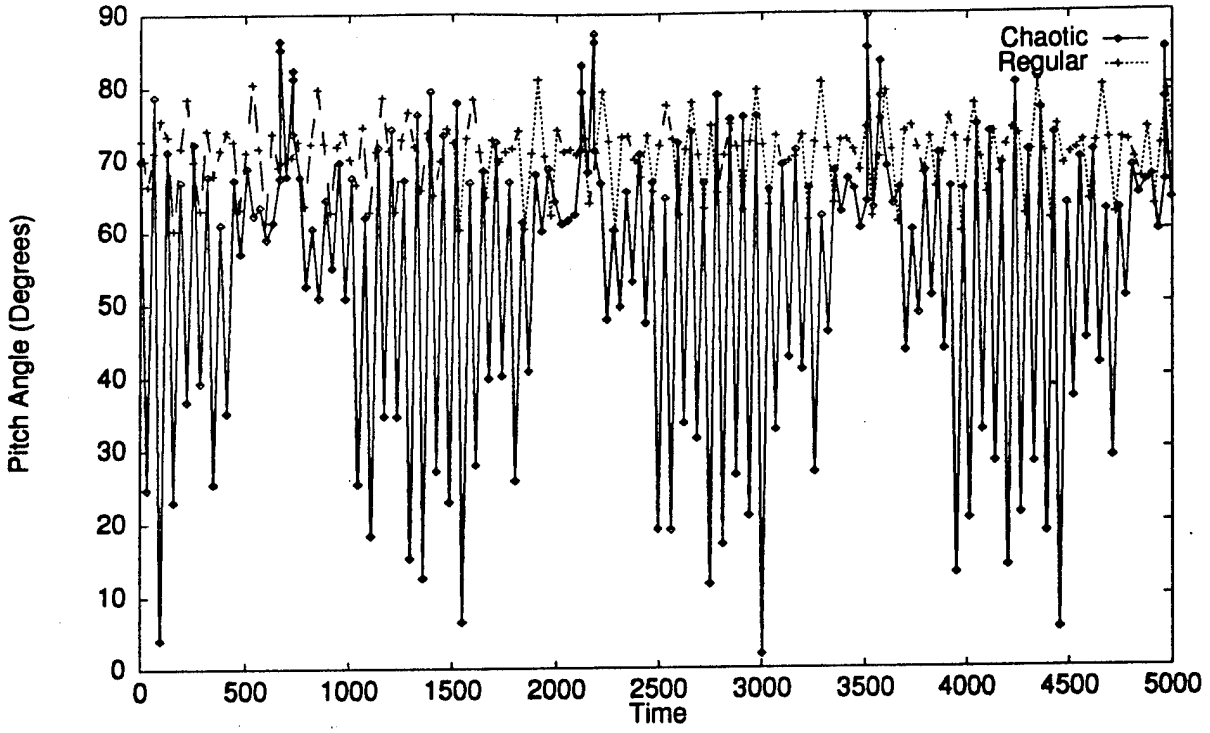

(c)

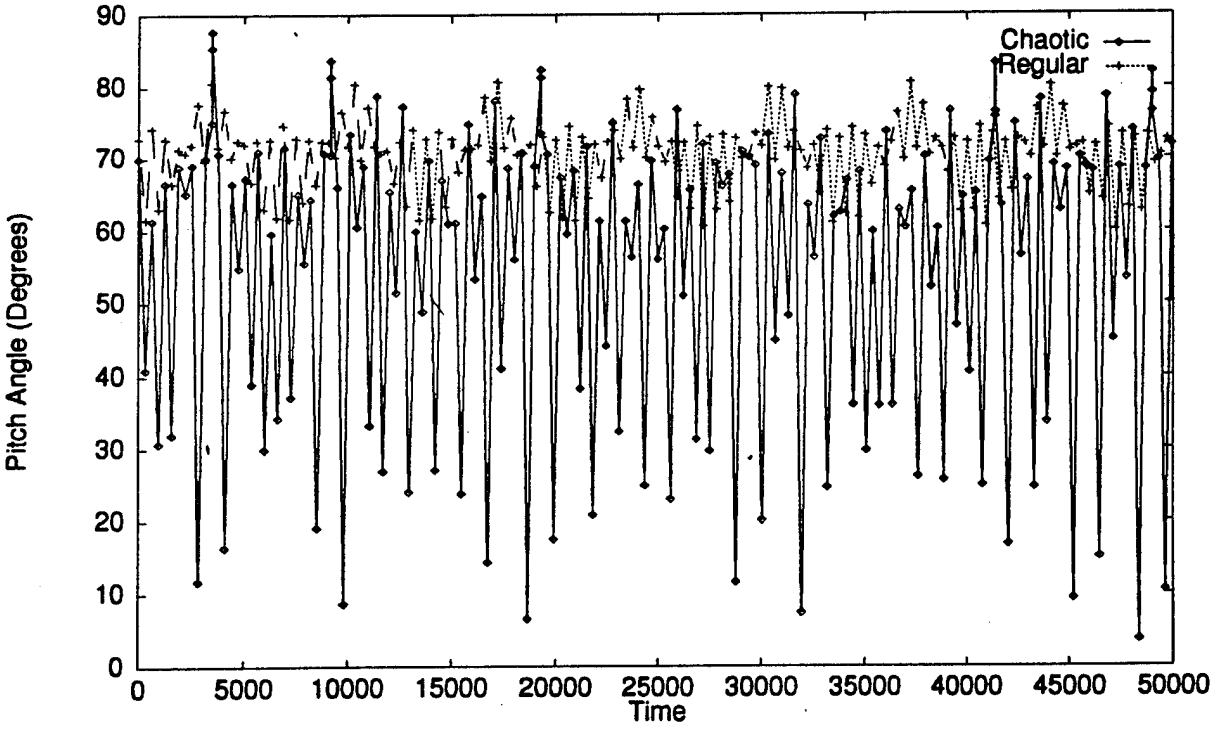

(d)

Figure 5 (c) and (d)

Functional dependence pitch angle at the geomagnetic equator on time for K=1, $\Omega = 2.333$, $Q_0 = z_0 = 0$, $\omega_b = 10^{-2}$ (c), and $\omega_b = 10^{-3}$ (d). The chaotic plot is for $\Omega_1 = 0.46$, $P_0 = 1.6$, and $p_{z0} = 0.46$, while the regular is for $\Omega_1 = 0.1$, $P_0 = 1.2$, and $p_{z0} = 0.27$. Both plots have $\alpha_0 \approx 70^\circ$.